Anharmonic Oscillator

CARL M. BENDER*†

Department of Physics, Harvard University, Cambridge, Massachusetts 02138

AND

TAI TSUN WU

Division of Engineering and Applied Physics, Harvard University, Cambridge, Massachusetts 02138

(Received 4 February 1969)

We consider the anharmonic oscillator defined by the differential equation $(-d^2/dx^2 + \frac{1}{4}x^2 + \frac{1}{4}\lambda x^4)\Phi(x)$ $= E(\lambda)\Phi(x)$ and the boundary condition $\lim_{x\to\pm\infty}\Phi(x) = 0$. This model is interesting because the perturbation series for the ground-state energy diverges. To investigate the reason for this divergence, we analytically continue the energy levels of the Hamiltonian H into the complex λ plane. Using WKB techniques, we find that the energy levels as a function of λ, or more generally of λ^α, have an infinite number of branch points with a limit point at $\lambda = 0$. Thus, the origin is not an isolated singularity. Level crossing occurs at each branch point. If we choose $\alpha = \frac{1}{3}$, the resolvent $(z-H)^{-1}$ has no branch cut. However, for all z it has an infinite sequence of poles which have a limit point at the origin. The anharmonic oscillator is of particular interest to field theoreticians because it is a model of $\lambda\varphi^4$ field theory in one-dimensional space-time. The unusual and unexpected properties exhibited by this model may give some indication of the analytic structure of a more realistic field theory.

I. INTRODUCTION

IN this paper, we discuss the familiar anharmonic oscillator.[1] We are concerned with the eigenvalue problem defined by the differential equation

$$(-d^2/dx^2 + \tfrac{1}{4}x^2 + \tfrac{1}{4}\lambda x^4)\Phi(x) = E(\lambda)\Phi(x) \quad (1.1)$$

and the associated boundary condition

$$\lim_{x\to\pm\infty} \Phi(x) = 0. \quad (1.2)$$

We propose to answer the following questions within the context of the anharmonic oscillator:

(i) Is the perturbation series for the ground-state energy, which is a power series in the coupling constant λ, convergent for any $\lambda \neq 0$?

(ii) If not, does the ground-state energy, considered as a function of complex λ or more generally as a func-

tion of some fractional power α of λ, have an isolated singularity at $\lambda = 0$?

(iii) Is the resolvent $(z-H)^{-1}$, considered as a function of λ^α for fixed z, analytic at $\lambda = 0$? If not, is the point $\lambda = 0$ an isolated singularity?

The answer to all these questions is *no*. More precisely, the energy levels, which are originally defined only for positive values of λ, can be analytically continued into the complex λ plane. This analytic continuation has an infinite number of branch points, which have a limit point at the origin $\lambda = 0$. Moreover, level crossing occurs at each branch point. If α is chosen to be $\frac{1}{3}$, the resolvent has no branch cut. However, for all z, $(z-H)^{-1}$ has an infinite number of poles which have a limit point at the origin. These qualitative analytic properties of the energy levels and of the resolvent were totally unexpected and are, we feel, most unusual and exciting.

This paper will adhere to the following outline: In Sec. II (and Appendices A–E), we inspect in great detail the properties of the perturbation series for the ground-state energy in our model. However, this direct inspection gives no clue as to the nature of the singularities in the λ plane which cause this divergence. To

---

[1] The techniques used in this paper to analyze the anharmonic oscillator were first introduced by C. M. Bender and T. T. Wu, Phys. Rev. Letters **21**, 406 (1968).

184   1231

understand these singularities better, in Sec. III, we analytically continue the energy levels into the λ plane and derive some exact properties of this continuation. In particular, we derive an exact condition which gives the locations of the singularities in the λ plane.

To apply this condition we must know the wave function in coordinate space. To calculate the wave function approximately, in Sec. IV, we present a technique using zeroth-order WKB methods in the complex plane. (In Appendix F, we make the calculation of the wave function more precise by using first-order WKB techniques.)

In Sec. V, we use the results of Sec. IV to determine the singularities of the resolvent. In Sec. VI (and Appendix G), we combine the results of Secs. III and IV to find the approximate locations of the singularities in the analytic continuation of the energy levels. Section VI contains an exhaustive qualitative description of the analytic continuation of the energy levels $E(\lambda)$. The major result of this paper is that the energy levels of the anharmonic oscillator for a given positive real λ are the positive real values of $E(\lambda)$ on each of the infinite number of branches of a Riemann surface. Each energy level corresponds to a sheet of this Riemann surface.

Although it is not necessary to understand any field theory to read this paper (aside from Appendices A–C), it is important to point out that the anharmonic oscillator is a simple model field theory in one-dimensional space-time. This field theory is defined by the Hamiltonian

$$H = \tfrac{1}{2}\dot{\varphi}^2 + \tfrac{1}{2}m^2\varphi^2 + \lambda\varphi^4 \qquad (1.3)$$

and the commutation relations

$$[\varphi, \dot{\varphi}] = i. \qquad (1.4)$$

[In Appendix A, we prove rigorously that Eqs. (1.1) and (1.2) are consequences of Eqs. (1.3) and (1.4). In fact, Eqs. (1.1) and (1.2) are the coordinate representation of H.]

Since this field-theory model involves no space dimensions, there are no asymptotic states and therefore no particle scattering. Also, there is only one degree of freedom. In fact, all this theory describes is a universe which sits at one point and oscillates. Nevertheless, this model has value to the field theoretician. It enables one to conjecture with slight supporting evidence[2] that many of the fascinating properties we have observed are also present in a more realistic field theory. This model may give us some idea of the vast underlying complexity of such a theory.

The model was originally chosen for study because it had a well-defined but divergent perturbation series. We believe that the divergence of perturbation series

in field theory was first discussed by Dyson.[3] Since then, many papers have been written on this topic. A particularly interesting investigation was carried out by Jaffe.[4] Jaffe proved that in two-dimensional space-time the perturbation series for Green's functions in self-interacting boson field theories diverge even though these series exist term by term. However, as far as we know, no techniques have been discovered to elucidate the singularities in field theories with divergent perturbation series. In this paper, we develop for the first time methods to describe the actual singularity structure of a particular field theory.

Having achieved the results of this paper, we hope in the future to apply the new analytical tools of Secs. III–VI to other models of increasing complexity in order to better understand how singularities depend upon the form of interaction. Additional zero-dimensional bose field theories which ought to be considered are self-interactions such as φ^6, φ^{2N}, and $\cos\varphi$ and couplings such as $\varphi_1^2\varphi_2^2$. Hopefully, these WKB techniques will be advanced to the point where they may be used to analyze higher-dimensional theories.

II. GROUND-STATE-ENERGY PERTURBATION SERIES

The perturbation series for the ground-state energy $E_0(\lambda)$ in this model is a power series in the coupling constant λ. This power series takes the form

$$E_0(\lambda) = \tfrac{1}{2}m + \sum_{n=1}^{\infty} mA_n(\lambda/m^3)^n. \qquad (2.1)$$

Two methods for calculating the A_n in this equation are discussed below. Each method reveals some important properties of Eq. (2.1).

Method 1. In general, in a field theory the perturbation series for the ground-state energy is the sum of all connected Feynman diagrams having no external legs. Hence, Feynman diagrams can be used to calculate the A_n. (As an illustration of Feynman-diagram techniques, we calculate A_1, A_2, and A_3 in Appendix B.)

Moreover, an integral representation for these Feynman diagrams provides upper and lower bounds on the terms A_n in the perturbation series. We outline below the procedure for estimating these upper and lower bounds. (Detailed proofs for the following statements are given in Appendix C.)

(i) From the form of the Feynman integral representation, it follows that in the perturbation series all diagrams with the same number of vertices add in phase.

(ii) The integral representation places *uniform* bounds on the contribution of each diagram having n vertices.

---

[2] A. M. Jaffe, in his thesis [Princeton University, 1965 (unpublished)], was able to analytically continue the resolvent for $\lambda\varphi^4$ field theories of any space dimension into the cut λ plane. Jaffe did not predict the properties of the resolvent when $|\arg\lambda| \geq 180°$ (off the first sheet) but, as far as he did predict, his work agrees with ours.

[3] F. J. Dyson, Phys. Rev. **85**, 631 (1952).

[4] A. M. Jaffe, Commun. Math. Phys. **1**, 127 (1965). This paper contains a very complete list of references.

(iii) The maximum and minimum number of diagrams with n vertices is found to be $(2n-1)!!8^n$ and $(n-1)!3^{-n}$.

Combining the above three results implies that $A_n(-1)^{n+1}$ are positive numbers bounded below and above by

$$A\Gamma(n)B^n < A_n(-1)^{n+1} < C\Gamma(\tfrac{5}{2}n)D^n, \qquad (2.2)$$

where A, B, C, and D are positive constants.[5] Equation (2.2) implies that, although the perturbation series [Eq. (2.1)] is finite in every order, the ground-state energy is not an analytic function of λ^α about $\lambda=0$ for any α.

Method 2. The A_n can also be calculated from a difference equation. To derive this difference equation we use the differential equation [Eq. (1.1)] which is

$$(-d^2/dx^2+\tfrac{1}{4}x^2+\tfrac{1}{4}\lambda x^4)\Phi(x)=E(\lambda)\Phi(x), \qquad (2.3)$$

and the boundary conditions [Eq. (1.2)]

$$\lim_{x\to\pm\infty}\Phi(x)=0. \qquad (2.4)$$

In Eq. (2.3), we substitute

$$\Phi(x)=\sum_{n=0}^{\infty}\lambda^n e^{-x^2/4}B_n(x), \qquad (2.5)$$

where $B_0=1$ and $B_n(x)$ are the polynomials in x to be determined for $n=1, 2, 3, \cdots$.

We then combine Eqs. (2.1), (2.3), and (2.5) to get

$$\sum_{n=0}^{\infty}\lambda^n[xB_n'(x)-B_n''(x)+\tfrac{1}{4}x^4B_{n-1}(x)]$$

$$=(\sum_{n=1}^{\infty}\lambda^n A_n)(\sum_{m=0}^{\infty}\lambda^m B_m(x)). \qquad (2.6)$$

Finally, we let $x=\sqrt{2}y$ and

$$B_i(y)=\sum_{j=1}^{2i}y^{2j}B_{i,j}(-1)^i. \qquad (2.7)$$

The result is

$$2jB_{i,j}=(j+1)(2j+1)B_{i,j+1}+B_{i-1,j-2}$$

$$-\sum_{p=1}^{i-1}B_{i-p,1}B_{p,j}. \qquad (2.8)$$

Equation (2.8) is the desired difference equation because the numbers $B_{i,j}$ are related to the A_n by the simple equation

$$A_n=-B_{n,1}. \qquad (2.9)$$

---

[5] If the Hamiltonian were Wick-ordered, there would be fewer diagrams of order n because a line could not have both ends connected to the same vertex. Thus, the terms in the Wick-ordered perturbation series would be slightly smaller than those of our non-Wick-ordered series. However, the estimate [Eq. (2.2)] would hold for both perturbation series.

Equation (2.8) was used on a computer to calculate the first 75 terms in the ground-state-energy perturbation series [Eq. (2.1)].[6] From these results we have determined that their detailed asymptotic growth is

$$A_n\sim(-1)^{n+1}(6/\pi^3)^{1/2}\Gamma(n+\tfrac{1}{2})3^n. \qquad (2.10)$$

[In Appendix D we discuss the details of this computer calculation and list the first 75 terms in the perturbation series to 12-place accuracy. In Appendix E, we present the calculation of Eq. (2.10).]

Numerical investigation of the difference equation [Eq. (2.8)] brings to light the following exact additional properties of the A_n which are not immediately evident from the Feynman-diagram treatment of the perturbation series:

(i) All A_n are rational fractions.

(ii) If we define

$$I_n\equiv(-1)^{n+1}4^n A_n, \qquad (2.11)$$

then the I_n are all positive *integers*.

(iii) Every integer I_n is divisible by 3.

We list below the first nine terms in the perturbation series in exact fraction form to illustrate the above characteristics of the A_n.

$$A_1=\tfrac{3}{4}, \qquad (2.12a)$$

$$A_2=-21/8, \qquad (2.12b)$$

$$A_3=333/16, \qquad (2.12c)$$

$$A_4=-30\ 885/128, \qquad (2.12d)$$

$$A_5=916\ 731/256, \qquad (2.12e)$$

$$A_6=-65\ 518\ 401/1024, \qquad (2.12f)$$

$$A_7=2\ 723\ 294\ 673/2048, \qquad (2.12g)$$

$$A_8=-1\ 030\ 495\ 099\ 053/32\ 768, \qquad (2.12h)$$

$$A_9=54\ 626\ 982\ 511\ 455/65\ 536. \qquad (2.12i)$$

III. ANALYTIC CONTINUATION OF ENERGY LEVELS

In Sec. II and associated appendices, we studied the properties of the ground-state-energy perturbation series [Eq. (2.1)]. However, this study did not reveal the reason for the divergence of the series. In other words, the singularity structure of $E_0(\lambda)$ in the complex λ plane is as yet unknown. In this section, we define the analytic continuation of the energy levels, which are the eigenvalues of the differential equation [Eq. (1.1)], into the λ plane. Then we present some heuristic derivations of some properties of this continuation.
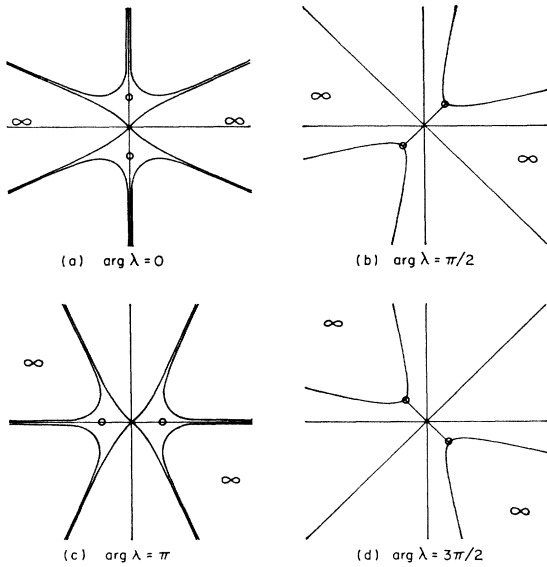

Fig. 1. Curves in the complex x plane where $\mathrm{Re}\lambda^{-1}[(1+\lambda x^2)^{1/2} -1]=0$ for various values of argλ. The circles denote the turning points at $x=\pm i\lambda^{-1/2}$. The symbol ∞ indicates the sectors in which the boundary condition [Eq. (3.4)] applies.

(a) arg $\lambda = 0$ (b) arg $\lambda = \pi/2$ (c) arg $\lambda = \pi$ (d) arg $\lambda = 3\pi/2$

We shall need only Eqs. (1.1) and (1.2) which are

$$(-d^2/dx^2+\tfrac{1}{4}x^2+\tfrac{1}{4}\lambda x^4)\Phi(x)=E(\lambda)\Phi(x) \qquad (3.1)$$

and

$$\lim_{x\to\pm\infty}\Phi(x)=0. \qquad (3.2)$$

Equations (3.1) and (3.2) yield the asymptotic behavior of $\Phi(x)$ for large $|x|$ along the real axis:

$$\Phi(x)\sim\exp(-\tfrac{1}{6}\lambda^{1/2}|x|^3). \qquad (3.3)$$

Equation (3.3) implies that Eq. (3.2), the boundary condition, holds not only on the real axis but also for complex x in the sector $|\arg x|<\tfrac{1}{6}\pi$.

Until now λ has been positive. When λ is complex, $\Phi(x)$ must satisfy the general boundary condition

$$\lim_{|x|\to\infty}\Phi(x)=0 \quad \text{when} \quad |\arg(\pm x)+(\tfrac{1}{6}\,\arg\lambda)|<\tfrac{1}{6}\pi, \qquad (3.4)$$

which follows from Eqs. (3.2) and (3.3).

We can now continue $E(\lambda)$ into the λ plane. We *define* the analytic continuation $E(\lambda)$ by the differential equation [Eq. (3.1)] in which $\Phi(x)$ satisfies the boundary condition in Eq. (3.4).

We shall use Eqs. (3.1) and (3.4) to find some exact properties of the analytic continuation of $E(\lambda)$:

Property (i). We may analytically continue $E(\lambda)$ to all points λ (except $\lambda=0$) where $\int_C \Phi^2(x,\lambda)dx\neq0$. The integral is taken along an appropriate path C in the complex x plane.

Proof. Normalize $\Phi(x)$ by choosing

$$\Phi(0,\lambda)=1 \text{ for an even-parity wave function} \qquad (3.5a)$$

and

$$(d/dx)\Phi(0,\lambda)=1 \text{ for an odd-parity}$$
$$\text{wave function}. \qquad (3.5b)$$

Vary λ by

$$\lambda\to\lambda+\delta\lambda. \qquad (3.6)$$

Then,

$$E(\lambda)\to E(\lambda)+\delta E(\lambda) \qquad (3.7)$$

and

$$\Phi(x,\lambda)\to\Phi(x,\lambda)+\delta\Phi(x,\lambda). \qquad (3.8)$$

$\delta\Phi$ has the property that

$$\delta\Phi(0,\lambda)=0 \quad \text{or} \quad \delta\Phi'(0,\lambda)=0$$

for even or odd parity, respectively. $\delta\Phi(x,\lambda)$ obeys the same boundary conditions at ∞ as $\Phi(x,\lambda)$ does, namely, Eq. (3.4).

Substituting Eqs. (3.6), (3.7), and (3.8) into Eq. (3.1) gives

$$(d^2/dx^2-\tfrac{1}{4}x^2-\tfrac{1}{4}\lambda x^4)\delta\Phi(x,\lambda)-\tfrac{1}{4}\delta\lambda x^4\Phi(x,\lambda)$$
$$=-E(\lambda)\delta\Phi(x,\lambda)+\delta E(\lambda)\Phi(x,\lambda). \qquad (3.9)$$

Multiply Eq. (3.9) by $\Phi(x,\lambda)$. Then integrate by parts along a path C in the complex x plane such that each end of the path goes to ∞ in a sector in which the boundary condition [Eq. (3.4)] applies. [See Fig. 1 for the location of the sectors in which Eq. (3.4) applies for various choices of argλ.] The result of this manipulation is

$$0=\tfrac{1}{4}\delta\lambda\int_C x^4\Phi^2(x,\lambda)dx-\delta E(\lambda)\int_C \Phi^2(x,\lambda)dx. \qquad (3.10)$$

Hence, $E(\lambda)$ is analytic (its derivative with respect to complex λ exists) at all points except those for which

$$\int_C \Phi^2(x,\lambda)dx=0. \qquad (3.11)$$

Equation (3.11) will be used in Sec. VI as a condition for determining the location of the singularities of $E(\lambda)$.

Property (ii). At points where $E(\lambda)$ is analytic, there is no degeneracy in the energy.

Proof. Suppose $\Phi_1(x,\lambda)$ and $\Phi_2(x,\lambda)$ are two linearly-independent wave-function solutions to Eq. (3.1) each associated with energy E. We find that the derivative of the Wronskian $W'[\Phi_1(x),\Phi_2(x)]$ vanishes. Hence the Wronskian W is a constant. Because Φ_1 and Φ_2 obey the boundary condition [Eq. (3.4)], the constant must be 0. A vanishing Wronskian implies that Φ_1 and Φ_2 are not linearly-independent. Hence there is no degeneracy.

Property (iii). If there is a point λ_0 in the λ plane where $E_1(\lambda)\to E_2(\lambda)$ as $\lambda\to\lambda_0$, then $E_1(\lambda)$ is singular at $\lambda=\lambda_0$.

Proof. If $\Phi_i(x,\lambda)$ are the wave functions associated with $E_i(\lambda)$ for $i=1$ and 2, then because of property (ii)

$\Phi_1(x,\lambda) \to \Phi_2(x,\lambda)$ as $\lambda \to \lambda_0$. Consider the equation

$$\Phi_1(x,\lambda)(-d^2/dx^2+\tfrac{1}{4}x^2+\tfrac{1}{4}\lambda x^4)\Phi_2(x,\lambda)$$
$$= E_2\Phi_1(x,\lambda)\Phi_2(x,\lambda). \quad (3.12)$$

Integrating Eq. (3.12) over the contour C in the complex x plane and integrating by parts gives

$$(E_1-E_2)\int_C \Phi_1(x,\lambda)\Phi_2(x,\lambda)dx=0. \quad (3.13)$$

Thus, when $\lambda\neq\lambda_0$,

$$\int_C \Phi_1(x,\lambda)\Phi_2(x,\lambda)dx=0. \quad (3.14)$$

Letting $\lambda \to \lambda_0$ in Eq. (3.14) gives

$$\int_C \Phi_2{}^2(x,\lambda)dx=0, \quad (3.15)$$

which is just Eq. (3.11). As a result of property (i), $E_1(\lambda)$ is singular at $\lambda=\lambda_0$. Thus, level crossing only occurs at singularity points of $E(\lambda)$.

Property (iv). The singularities of $E(\lambda)$ are of the square-root type for $\lambda\neq0$.

Proof. Suppose $E(\lambda)$ has a singularity at $\lambda=\lambda_0\neq0$. Let

$$\epsilon= (\lambda-\lambda_0)^{1/2}. \quad (3.16)$$

Then,

$$(-d^2/dx^2+\tfrac{1}{4}x^2+\tfrac{1}{4}\lambda_0 x^4+\tfrac{1}{4}\epsilon^2 x^4)\Phi(x,\epsilon) = E(\epsilon)\Phi(x,\epsilon). \quad (3.17)$$

Expand

$$\Phi(x,\epsilon)=\Phi_0(x)+\epsilon\Phi_1(x)+\epsilon^2\Phi_2(x)+\cdots \quad (3.18)$$

and

$$E(\epsilon)=\alpha+\epsilon\beta+\epsilon^2\gamma+\cdots. \quad (3.19)$$

If we let $\Theta(x) = -d^2/dx^2+\tfrac{1}{4}x^2+\tfrac{1}{4}\lambda_0 x^4$, then

$$\Theta(x)\Phi_0(x)=\alpha\Phi_0(x), \quad (3.20a)$$

$$\Theta(x)\Phi_1(x)=\alpha\Phi_1(x)+\beta\Phi_0(x), \quad (3.20b)$$

and

$$\Theta(x)\Phi_2(x)+\tfrac{1}{4}x^4\Phi_0(x)=\alpha\Phi_2(x)$$
$$+\beta\Phi_1(x)+\gamma\Phi_0(x). \quad (3.20c)$$

Equation (3.20b) gives no useful information, but multiplying Eq. (3.20c) by $\Phi_0(x)$ and integrating gives

$$\beta=\int_C \tfrac{1}{4}x^4\Phi_0{}^2(x)dx \Big/ \int_C \Phi_1(x)\Phi_0(x)dx. \quad (3.21)$$

β exists if the denominator in Eq. (3.21) does not vanish[7]; that is,

$$\int_C \Phi_1(x)\Phi_0(x)dx\neq0. \quad (3.22)$$

---

[7] To zeroth order in the WKB expansion discussed in Secs. IV and VI, it can be shown that for those points which satisfy Eq. (3.11), Eq. (3.22) is indeed true. If Eq. (3.22) were not true, we

An argument similar to the one given in the proof of property (i) implies that λ_0 is a square-root-type singularity point of $E(\lambda)$. Since a square-root singularity has associated with it a double Riemann sheet, energy-level crossing must take place at all points $\lambda_0\neq0$ satisfying Eq. (3.11).

IV. WKB SOLUTION

In this section, we shall approximate the wave function $\Phi(x)$ using zeroth-order WKB techniques.[8] We only consider the case where $|\lambda|$ is small. We will need Eqs. (1.1) and (1.2) which are

$$(-d^2/dx^2+\tfrac{1}{4}x^2+\tfrac{1}{4}\lambda x^4)\Phi(x)=E(\lambda)\Phi(x) \quad (4.1)$$

and

$$\lim_{x\to\pm\infty} \Phi(x)=0. \quad (4.2)$$

The zeroth-order WKB solution to Eq. (4.1) is[8]

$$\Phi=\text{const}\times\mu^{-1/2} \exp\left(\pm\int^x \mu(x)dx\right), \quad (4.3)$$

where

$$\mu(x)=[-E(\lambda)+\tfrac{1}{4}x^2+\tfrac{1}{4}\lambda x^4]^{1/2}. \quad (4.4)$$

For large $|x|$, Eq. (4.3), the zeroth-order WKB solution, becomes

$$\Phi(x)\sim\text{const}\times (x^2+\lambda x^4)^{-1/4}$$
$$\times\exp\{(-6\lambda)^{-1}[(1+\lambda x^2)^{3/2}-1]\}. \quad (4.5)$$

Given $\arg\lambda$, we use Eq. (4.5) to locate in the complex x plane the turning points and the sectors in which the general boundary condition [Eq. (3.4)] applies. The turning points are at $\pm i\lambda^{-1/2}$. The boundaries of the above sectors are curves given by

$$\text{Re}\{\lambda^{-1}[(1+\lambda x^2)^{3/2}-1]\}=0.$$

The sectors and turning points are plotted in Fig. 1 for $\arg\lambda=0$, $\tfrac{1}{2}\pi$, π, and $\tfrac{3}{2}\pi$.

We now begin the WKB analysis. Near the origin $x=0$, the differential equation [Eq. (4.1)] becomes

$$(d^2/dx^2+E-\tfrac{1}{4}x^2)\Phi(x)=0, \quad (4.6)$$

which is the defining equation for the parabolic cylinder function $D_{E-\frac{1}{2}}(x)$.[9] The correct physical solution to Eq. (4.6) is

$$\Phi(x)=C[D_{E-\frac{1}{2}}(x)\pm D_{E-\frac{1}{2}}(-x)] \quad (4.7)$$

---

would have to reexpand $E(\lambda)$ and $\Phi(x,\lambda)$ in terms of $(\lambda-\lambda_0)^{1/3}=\epsilon$. Physically, this would mean that three energy levels cross at λ_0 instead of two as is the case. One would expect intuitively that the chance of three levels crossing at the same point λ_0 is small.

[8] For a review of zeroth-order WKB techniques, see A. Messiah, *Quantum Mechanics* (John Wiley & Sons, Inc., New York, 1961), Vol. 1, pp. 232–233. For a discussion of WKB techniques in the complex plane see T. T. Wu, Phys. Rev. **143**, 1110 (1966).

[9] A. Erdélyi, W. Magnus, F. Oberhettinger, and F. G. Tricomi, *Bateman Manuscript Project* (McGraw-Hill Book Co., New York, 1953), Vol. 2, pp. 116–123. In the future we will refer to this reference as BMP.

for even- or odd-parity wave functions. C is a multiplicative constant.

When the phase of λ is less than 270°, we can asymptotically connect the parabolic cylinder function in Eq. (4.7) to the WKB solution in Eq. (4.5). The connection restricts the possible values of E to

$$E = 2n + \tfrac{1}{2} \quad \text{for even parity} \tag{4.8a}$$

and

$$E = 2n + \tfrac{3}{2} \quad \text{for odd parity}, \tag{4.8b}$$

where $n = 0, 1, 2, \cdots$.

However, Eq. (4.7) cannot be directly connected to Eq. (4.5) when the phase of λ is near 270° because a turning point lies in the path of the connection [see Fig. 1(d)]. Instead, we use the following procedure:

We define new variables $r \equiv xe^{i\pi/4}$, $\rho \equiv \lambda e^{-3\pi i/2}$, and $\epsilon \equiv 4iE$. In terms of these variables, Eq. (4.1) becomes

$$[d^2/dr^2 + \tfrac{1}{4}(-\epsilon + r^2 - \rho r^4)]\Phi(r) = 0. \tag{4.9}$$

We assume that $|\lambda|$ is so small that $|\rho\epsilon| \ll 1$.
We define

$$r_0 \equiv \{[1 - (1 - 4\rho\epsilon)^{1/2}](2\rho)^{-1}\}^{1/2} \sim \epsilon^{1/2} \tag{4.10a}$$

and

$$r_1 \equiv \{[1 + (1 - 4\rho\epsilon)^{1/2}](2\rho)^{-1}\}^{1/2} \sim \rho^{-1/2}. \tag{4.10b}$$

r_1 is approximately the position of the turning point. $|\rho\epsilon| \ll 1$ implies that $|r_0| \ll |r_1|$.

Next, we identify four regions in the complex x plane: region A in which r is near the origin, $0 < |r| \ll |r_0| \ll |r_1|$; region B in which $|r| \ll |r_1|$ but $|r| \gg |r_0|$; region C in which r is near the turning point, $|r| \lesssim |r_1|$ but $|r| \gg |r_0|$; and region D in which r is at the turning point, $|r| \sim |r_1|$.

In order to carry out the WKB procedure when $\arg\lambda$ is near 270°, approximate solutions to Eq. (4.9) must be found in regions A, B, C, and D. Then these solutions must be connected asymptotically at the boundaries of the regions.

Region A. In region A, Eq. (4.9) becomes approximately (that is, to zeroth order in λ)

$$(d^2/dr^2 - \tfrac{1}{4}\epsilon - \tfrac{1}{4}r^2)\Phi_A(r) = 0. \tag{4.11}$$

Equation (4.11) is the transformed defining equation for a parabolic cylinder function.[9] The even-parity solution to this equation is

$$\Phi_A(r) = C[D_{-\frac{1}{2}-i\epsilon/4}(re^{-i\pi/4}) + D_{-\frac{1}{2}-i\epsilon/4}(-re^{-i\pi/4})]. \tag{4.12}$$

(In this section, we will treat even-parity wave functions in detail; only the final results will be given for odd-parity solutions.)

To compute the asymptotic expansion of Φ_A in region A, we need the leading term in the asymptotic expansion of $D_\nu(z)$,[9] which is

$$D_\nu(z) \sim z^\nu e^{-\frac{1}{4}z^2} \quad \text{for } -\tfrac{3}{4}\pi < \arg z < \tfrac{3}{4}\pi \tag{4.13a}$$

and

$$D_\nu(z) \sim z^\nu e^{-\frac{1}{4}z^2} - [(2\pi)^{1/2}/\Gamma(-\nu)]e^{\nu\pi i}z^{-\nu-1}e^{\frac{1}{4}z^2}$$

$$\text{for } \tfrac{1}{4}\pi < \arg z < (5/4)\pi. \tag{4.13b}$$

Equation (4.13) yields the asymptotic behavior of $\Phi_A(r)$ in region A for large $|r|$; that is, for r near region B. After much algebraic manipulation we have the desired asymptotic expansion:

$$\Phi_A(r) \sim \frac{C_1}{\sqrt{r}} \left\{ \frac{1}{\Gamma(\tfrac{1}{4} - \tfrac{1}{8}i\epsilon)} \exp[\tfrac{1}{4}i(r^2 - \epsilon \ln r + \tfrac{1}{2}\epsilon \ln 2 - \tfrac{1}{2}\pi)] \right.$$

$$\left. + \frac{1}{\Gamma(\tfrac{1}{4} + \tfrac{1}{8}i\epsilon)} \exp[-\tfrac{1}{4}i(r^2 - \epsilon \ln r + \tfrac{1}{2}\epsilon \ln 2 - \tfrac{1}{2}\pi)] \right\}, \tag{4.14}$$

where

$$C_1 = \frac{C 2\pi e^{\pi\epsilon/16} 2^{-i\epsilon/8}}{\Gamma(\tfrac{3}{4} + \tfrac{1}{8}i\epsilon)}. \tag{4.15}$$

Region B. In regions B and C, we need the zeroth-order WKB solution[8] to Eq. (4.9) which is

$$\Phi_{\text{WKB}}(x) = (-\epsilon + r^2 - \rho r^4)^{-1/4}$$

$$\times \left\{ C_2 \exp\left[\tfrac{1}{2}i \int_{r_0}^{r} (-\epsilon + r^2 - \rho r^4)^{1/2} dr\right] \right.$$

$$\left. + C_3 \exp\left[-\tfrac{1}{2}i \int_{r_0}^{r} (-\epsilon + r^2 - \rho r^4)^{1/2} dr\right] \right\}. \tag{4.16}$$

In Eq. (4.16), we choose to integrate from the reference point r_0. We are free to choose the reference point, but this choice must be maintained for the WKB solution in region C as well as in region B.

For r in region B, the choice of r_0 and r_1 in Eq. (4.10) allows us to simplify Eq. (4.16). To zeroth order in ρ,

$$(-\epsilon + r^2 - \rho r^4) \sim r^2 - \epsilon. \tag{4.17}$$

Using Eq. (4.17), we easily evaluate the integrals and expand the expression in front of the curly brackets in Eq. (4.16). The result is

$$\Phi_B(x) \sim (1/\sqrt{r})\{C_2 \exp[\tfrac{1}{4}i(r^2 - \epsilon \ln r - \tfrac{1}{2}\epsilon + \epsilon \ln(\tfrac{1}{2}\sqrt{\epsilon}))]$$

$$+ C_3 \exp[-\tfrac{1}{4}i(r^2 - \epsilon \ln r - \tfrac{1}{2}\epsilon + \epsilon \ln(\tfrac{1}{2}\sqrt{\epsilon}))]\}. \tag{4.18}$$

Region C. In region C, we need the zeroth-order WKB solution [Eq. (4.16)] to Eq. (4.9). The WKB solution in region C has the same constants C_2 and C_3 as the solution in region B. However, the integrals for region C are more difficult to perform than those for region B because of the approximations associated with region C which are $|r_0| \ll |r| \lesssim |r_1|$. We use the following

decomposition to evaluate the integrals:

$$\frac{1}{2}i \int_{r_0}^{r} dr(-\epsilon+r^2-\rho r^4)^{1/2}$$

$$=-\frac{1}{2}i\rho^{1/2}\int_{r}^{r_1}\left[(r^2-r_0^2)(r_1^2-r^2)\right]^{1/2}dr$$

$$+\frac{1}{2}i\rho^{1/2}\int_{r_0}^{r_1}\left[(r^2-r_0^2)(r_1^2-r^2)\right]^{1/2}dr. \quad (4.19)$$

To do the first integral, we introduce a change of variables

$$R=r_1-r. \quad (4.20)$$

Then, the integral becomes

$$-\frac{1}{2}i\rho^{1/2}(2r_1)^{1/2}(r_1^2-r_0^2)^{1/2}\int_0^R R^{1/2}dR$$

$$\sim-i3^{-1}2^{1/2}\rho^{-1/4}R^{3/2}. \quad (4.21)$$

In the second integral (the definite integral), we let $K^2=1-r_0^2 r_1^{-2}$. Then,

$$\frac{1}{2}i\rho^{1/2}\int_{r_0}^{r_1}\left[(r^2-r_0^2)(r_1^2-r^2)\right]^{1/2}dr$$

$$=\frac{1}{6}ir_1^3\left[(1+r_0^2 r_1^{-2})E(k)-2r_0^2 r_1^{-2}K(k)\right]. \quad (4.22)$$

$E(k)$ and $K(k)$ are the standard elliptic integrals.[10] Expanding $E(k)$ and $K(k)$ for k near 1 gives[11]

$$E(k)\sim1+\frac{r_0^2}{4r_1^2}\left(4\ln2-1-2\ln\frac{r_0}{r_1}\right) \quad (4.23a)$$

and

$$K(k)\sim\ln(4r_1/r_0). \quad (4.23b)$$

Thus,

$$\frac{1}{2}i\rho^{1/2}\int_{r_0}^{r_1}dr\left[(r^2-r_0^2)(r_1^2-r^2)\right]^{1/2}$$

$$\sim\frac{i}{6\rho}-\frac{1}{8}i\epsilon\left[\ln\frac{1}{\rho\epsilon}+4\ln2+1\right]. \quad (4.24)$$

We also note that

$$(-\epsilon+r^2-\rho r^4)^{-1/4}\sim\rho^{-1/4}(r_1^2-r_0^2)^{-1/4}(2r_1)^{-1/4}R^{-1/4}$$

$$\sim2^{-1/4}\rho^{1/8}R^{-1/4}. \quad (4.25)$$

Equations (4.19)–(4.25) imply that near the turning point the WKB solution [Eq. (4.16)] in region C is

----

[10] BMP, Vol. 2, pp. 317–318.
[11] To expand $E(k)$ and $K(k)$ near $k=1$, we use

$E(k)=\frac{1}{2}\pi\,_2F_1(-\frac{1}{2},\frac{1}{2};1;k^2)$ and $K(k)=\frac{1}{2}\pi\,_2F_1(\frac{1}{2},\frac{1}{2};1;k^2)$.

[See BMP, Vol. 2, p. 318, Eqs. (5) and (6).] Then we consult BMP, Vol. 1, p. 110, Eq. (12), where we find the appropriate expansion for the hypergeometric functions. These expansions may be simplified by using BMP, Vol. 1, pp. 1–20.

asymptotically

$$\Phi_C(r)\sim2^{-1/4}\rho^{1/8}R^{-1/4}\left\{C_2\exp\left[-\frac{1}{3}i\sqrt{2}\rho^{-1/4}R^{3/2}\right.\right.$$

$$\left.+\frac{i}{6\rho}-\frac{1}{8}i\epsilon\left(\ln\frac{1}{\rho\epsilon}+4\ln2+1\right)\right]$$

$$+C_3\exp\left[+\frac{1}{3}i\sqrt{2}\rho^{-1/4}R^{3/2}\right.$$

$$\left.\left.-\frac{i}{6\rho}+\frac{1}{8}i\epsilon\left(\ln\frac{1}{\rho\epsilon}+4\ln2+1\right)\right]\right\}. \quad (4.26)$$

Region D. In region D, we use Eq. (4.20) to change variables from r to R in the differential equation [Eq. (4.9)] and find that to zeroth order in ρ

$$(d^2/dR^2+\frac{1}{2}R\rho^{-1/2})\Phi_D(R)=0. \quad (4.27)$$

Equation (4.27) is an Airy differential equation.[12] The solution to Eq. (4.27) is

$$\Phi_D(R)=D(\frac{1}{3}y)^{1/2}K_{1/3}(2y^{3/2}), \quad (4.28)$$

where

$$y=-(18\sqrt{\rho})^{-1/3}R. \quad (4.29)$$

There is only one undetermined constant D in Eq. (4.28) because only the $K_{1/3}$ function obeys the general boundary conditions at ∞ [Eq. (3.4)].

To determine the behavior of $K_{1/3}(2y^{3/2})$ near the turning point, we note that[13]

$$K_{1/3}(2e^{3\pi i/2}(-y)^{3/2})=-\frac{1}{2}i\pi\{e^{i\pi/6}H_{1/3}{}^{(1)}(2(-y)^{3/2})$$

$$+e^{-i\pi/6}H_{1/3}{}^{(2)}(2y^{3/2})\}. \quad (4.30)$$

Then we use the asymptotic expansions[14] for $H^{(1)}$ and $H^{(2)}$ and find that in region D near the turning point

$$\Phi_D\sim C_4 R^{-1/4}[\exp(\frac{1}{3}i\sqrt{2}\rho^{-1/4}R^{3/2}-\frac{1}{4}i\pi)$$

$$+\exp(-\frac{1}{3}i\sqrt{2}\rho^{-1/4}R^{3/2}+\frac{1}{4}i\pi)], \quad (4.31)$$

where

$$C_4=D\pi^{1/2}3^{-1/3}2^{-11/12}\rho^{1/24}. \quad (4.32)$$

We have thus completed the determination of the asymptotic behavior of Φ in regions A, B, C, and D. Next we must connect Φ across regions A and B and across C and D. (Φ in region B is already connected to Φ in region C because the same WKB solution is used in both regions.) Connecting Eq. (4.14) in region A to Eq. (4.18) in region B and Eq. (4.26) in region C to Eq. (4.31) in region D gives two independent determinations of the ratio C_2/C_3. These are, respectively,

$$\frac{C_2}{C_3}=\frac{\Gamma(\frac{1}{4}+\frac{1}{8}i\epsilon)}{\Gamma(\frac{1}{4}-\frac{1}{8}i\epsilon)}\exp\left[\frac{i}{2}\left(\frac{\epsilon}{2}+\frac{\epsilon}{2}\ln\frac{8}{\epsilon}-\frac{\pi}{2}\right)\right] \quad (4.33a)$$

and

$$\frac{C_2}{C_3}=\exp\left[i\left(\frac{\pi}{2}-\frac{1}{3\rho}+\frac{\epsilon}{4}\ln\frac{16}{\rho\epsilon}+\frac{\epsilon}{4}\right)\right]. \quad (4.33b)$$

----

[12] BMP, Vol. 2, p. 22.
[13] BMP, Vol. 2, p. 5, Eq. (15) and p. 80, Eq. (43).
[14] BMP, Vol. 2, p. 85, Eqs. (1) and (2).

Combining Eqs. (4.33a) and (4.33b) gives a single transcendental equation which contains ρ and ϵ only.

$$\frac{\Gamma(\frac{1}{4}-\frac{1}{8}i\epsilon)}{\Gamma(\frac{1}{4}+\frac{1}{8}i\epsilon)}=\exp\left[\frac{5i\pi}{4}+\frac{i}{3\rho}+\frac{i\epsilon}{4}\ln\frac{\rho}{2}\right]. \quad (4.34)$$

Because Φ_D goes exponentially to 0 at ∞ as required by Eq. (4.5), we have connected the origin to ∞ via regions A, B, C, and D. We have found that Eq. (4.34) is the one requirement which must be obeyed for this connection to be valid. One should note that since Eq. (4.9) is a second-order differential equation, there are two undetermined constants in each region A, B, C, and D. An equation such as Eq. (4.34) is posible only because parity considerations restrict Φ_A to one constant C_1 and the boundary conditions [Eq. (3.4)] at ∞ limit Φ_D to one constant C_4.

If we rewrite Eq. (4.34) in terms of E instead of ϵ, we get

$$\frac{\Gamma(\frac{1}{4}+\frac{1}{2}E)}{\Gamma(\frac{1}{4}-\frac{1}{2}E)}=\exp\left(\frac{i}{3\rho}+\frac{5\pi i}{4}-E\ln\frac{\rho}{2}\right). \quad (4.35a)$$

For odd-parity wave functions the equivalent result is

$$\frac{\Gamma(\frac{3}{4}+\frac{1}{2}E)}{\Gamma(\frac{3}{4}-\frac{1}{2}E)}=\exp\left(\frac{i}{3\rho}-\frac{5\pi i}{4}-E\ln\frac{\rho}{2}\right). \quad (4.35b)$$

We may regard these results as approximate equations to zeroth order in λ relating the low-lying energy levels to complex λ near $\arg\lambda=270°$.

Appendix F contains a WKB calculation similar to the calculation in this section but to first order in λ. The result of Appendix F is more precise than Eq. (4.35), but it reduces to Eq. (4.35) when terms to first order in λ are neglected.

V. RESOLVENT

As a simple application of Eq. (4.35), we calculate in this section the locations of the singularities of the resolvent of the Hamiltonian H [Eq. (1.3)]. The resolvent of the Hamiltonian is conventionally defined as $(z-H)^{-1}$. We will prove that $(z-H)^{-1}$ has poles when $\arg\lambda$ is near 270°.

It is clear that $(z-H)^{-1}$ has a pole in the λ plane whenever the following equations are satisfied:

$$\frac{\Gamma(\frac{1}{4}+\frac{1}{2}z)}{\Gamma(\frac{1}{4}-\frac{1}{2}z)}=e^{5\pi i/4}e^{i/3\rho}e^{-z\ln(\rho/2)} \quad (5.1a)$$

for even parity;

$$\frac{\Gamma(\frac{3}{4}+\frac{1}{2}z)}{\Gamma(\frac{3}{4}-\frac{1}{2}z)}=e^{-5\pi i/4}e^{i/3\rho}e^{-z\ln(\rho/2)} \quad (5.1b)$$

for odd parity.

We solve each of the above equations separately for ρ by taking the logarithm of both sides. Given z, it is

always possible to choose a sufficiently small $|\rho|$ so that the $i/3\rho$ term dominates the $z\ln(2/\rho)$ term. Thus, the resolvent has poles at

$$\lambda=e^{3\pi i/2}\left[-3i\ln\frac{\Gamma(\frac{1}{4}+\frac{1}{2}z)}{\Gamma(\frac{1}{4}-\frac{1}{2}z)}+6\pi N+\frac{1}{4}\pi\right]^{-1}, \quad (5.2a)$$

provided that z is not an even integer $+\frac{1}{2}$, and at

$$\lambda=e^{3\pi i/2}\left[-3i\ln\frac{\Gamma(\frac{3}{4}+\frac{1}{2}z)}{\Gamma(\frac{3}{4}-\frac{1}{2}z)}+6\pi N-\frac{1}{4}\pi\right]^{-1}, \quad (5.2b)$$

provided that z is not an odd integer $+\frac{1}{2}$. In Eq. (5.2), N is any sufficiently large positive integer.

Equation (5.2) implies that for both parities $(z-H)^{-1}$ has an infinite sequence of poles approaching the origin. These correspond to an infinite sequence of choices for large positive N.

That the resolvent has poles was a surprise to us and, as far as we know, this had not even been conjectured. Jaffe[2] has proved that for negative z the resolvent is analytic in the cut λ plane, the cut extending from the origin to $-\infty$ along the negative real axis. This is entirely consistent with our results which maintain that no singularities appear in the resolvent until the phase of the coupling constant reaches nearly $\pm 270°$. Since the analytic continuation of the resolvent disappears through Jaffe's cut at $\arg\lambda=180°$, Jaffe observed no singularities.

VI. QUALITATIVE DESCRIPTION OF $E(\lambda)$

In this section, we use the results of Secs. III and IV to discover the properties of the analytic continuation of the energy levels $E(\lambda)$ as a function of complex λ. For purposes of clarity, this section is divided into three parts. Part A gives a calculation of the locations in the λ plane of the branch points of $E(\lambda)$. Part B describes in detail the paths traced out by the energy levels in the complex E plane as λ moves about the complex λ plane. Part C contains a discussion of level crossing.

A. Locations of Branch Points

We find the coordinates in the λ plane of the branch points of $E(\lambda)$ by solving a pair of simultaneous equations. The first of these is Eq. (4.35) which resulted from matching the zeroth-order WKB solution across the boundaries of regions A, B, C, and D, as was done in Sec. IV. We repeat Eq. (4.35) here:

$$\frac{\Gamma(\frac{1}{4}+\frac{1}{2}E)}{\Gamma(\frac{1}{4}-\frac{1}{2}E)}=\exp\left(\frac{i}{3\rho}+\frac{5\pi i}{4}-E\ln\frac{\rho}{2}\right)$$

for even parity, (6.1a)

$$\frac{\Gamma(\frac{3}{4}+\frac{1}{2}E)}{\Gamma(\frac{3}{4}-\frac{1}{2}E)}=\exp\left(\frac{i}{3\rho}-\frac{5\pi i}{4}-E\ln\frac{\rho}{2}\right)$$

for odd parity. (6.1b)

The second of the simultaneous equations is obtained by explicitly performing the integral in Eq. (3.11) which is

$$0 = \int_C dx\, \Phi^2(x,\lambda). \tag{6.2}$$

Equation (6.2) is an exact condition which is satisfied by those λ and only those λ which are branch points of $E(\lambda)$. Now that the approximate WKB wave function is known from Sec. IV, it is possible to evaluate this integral and in turn to use the result to find the branch points. The evaluation is very lengthy and is done in Appendix G. The result of this calculation is

$$0 = -\psi(E+\tfrac{1}{2}) + \frac{\pi}{2}\cot\left(\frac{1}{4}-\frac{E}{2}\right)\pi + \ln\frac{4}{\rho}$$

for even parity   (6.3a)

and

$$0 = -\psi(E+\tfrac{1}{2}) + \frac{\pi}{2}\cot\left(\frac{3}{4}-\frac{E}{2}\right)\pi + \ln\frac{4}{\rho}$$

for odd parity,   (6.3b)

where ψ is the logarithmic derivative of the Γ function. Equation (6.3) now embodies the condition for λ to be a singularity of $E(\lambda)$. Because Eqs. (6.3) and (6.1) are both correct to zeroth order in λ and since these are the pair of simultaneous equations that will be solved to find the singularities of $E(\lambda)$, the positions of the singularities will be known to zeroth order in λ.

Equations (6.1) and (6.3) must be put into a form favorable for simultaneous solution. To do so we use the following procedure:

(i) In this calculation, we consider $|\rho|$ to be small and $\arg\rho$ to be near $0°$ (because $\arg\lambda$ is near $270°$). We may express this by

$$\mathrm{Re}(1/\rho) = O(\Lambda) \tag{6.4a}$$

and

$$\mathrm{Im}(1/\rho) = O(\ln\Lambda), \tag{6.4b}$$

where Λ is very large.

(ii) We also consider only low-lying energy levels (that is, levels near the ground state) because the derivation of Eq. (6.1) in Sec. IV is valid only for such levels. We may express this by

$$|E| = O(1). \tag{6.5}$$

(iii) Define η by

$$E = 2n + \tfrac{1}{2} + \eta \quad \text{for even parity} \tag{6.6a}$$

and

$$E = 2n + \tfrac{3}{2} + \eta \quad \text{for odd parity}, \tag{6.6b}$$

where $n = 0, 1, 2, \cdots$.

(iv) Take the logarithm of both sides of Eq. (6.1), substitute Eq. (6.6), and apply the Legendre duplica-

tion formula[15] to get

$$\ln\Gamma(-n-\tfrac{1}{2}\eta) - \ln\Gamma(n+\tfrac{1}{2}\eta) + \ln\Gamma(2n+\eta) + \ln(2\sqrt{\pi})$$
$$-(2n+\eta)\ln 2 = \frac{i}{3\rho} + \frac{5\pi i}{4} - E\ln\frac{\rho}{2} - 2\pi Ni \tag{6.7a}$$

and

$$\ln\Gamma(-n-\tfrac{1}{2}\eta) - \ln\Gamma(n+\tfrac{1}{2}\eta) + \ln\Gamma(2n+\eta) + \ln(2\sqrt{\pi})$$
$$-(2n+\eta)\ln 2 + \ln(\tfrac{1}{2}+n+\tfrac{1}{2}\eta)$$
$$= \frac{i}{3\rho} - \frac{5\pi i}{4} - E\ln\frac{\rho}{2} - 2\pi Ni. \tag{6.7b}$$

N in this equation is an integer referring to the multiple-valued logarithmic function.

(v) Expand the $\ln\Gamma$ functions using[16]

$$\ln\Gamma(1+z) = -\gamma z + \sum_{m=2}^{\infty} (-1)^m \xi(m)(z^m/m). \tag{6.8}$$

The result is

$$\ln(\tfrac{1}{2}\eta) + \ln(2n)! + \tfrac{1}{2}\ln(2\pi) + \eta\left(-\gamma + \sum_{k=1}^{2n}\frac{1}{k}\right)$$
$$+\sum_{m=2}^{\infty}\frac{(-1)^m\eta^m}{m}\left\{\xi(m) - \xi(m)\left[\frac{1}{2^m} + \frac{1}{(-2)^m}\right] - \sum_{k=1}^{2n}\frac{1}{k^m}\right\}$$
$$= \frac{i}{3\rho} + \frac{\pi i}{4} - (n\pi i) - 2\pi Ni - (2n+\eta+\tfrac{1}{2})\ln\frac{\rho}{4} \tag{6.9a}$$

and

$$\ln(\tfrac{1}{2}\eta) + \ln(2n+1)! + \tfrac{1}{2}\ln(2\pi) + \eta\left(-\gamma + \sum_{k=1}^{2n+1}\frac{1}{k}\right)$$
$$+\sum_{m=2}^{\infty}\frac{(-1)^m\eta^m}{m}\left\{\xi(m) - \xi(m)\left[\frac{1}{(2)^m} + \frac{1}{(-2)^m}\right] - \sum_{k=1}^{2n+1}\frac{1}{k^m}\right\}$$
$$= \frac{i}{3\rho} + \frac{\pi i}{4} - (n\pi i) - 2\pi(N+1)i - (2n+\eta+\tfrac{3}{2})\ln\frac{\rho}{4}. \tag{6.9b}$$

(vi) Substitute Eq. (6.6) into Eq. (6.3) and expand the function using[17]

$$\psi(1+z) = -\gamma + \sum_{m=2}^{\infty} (-1)^m \xi(m) z^{m-1}. \tag{6.10}$$

The result is

$$\frac{1}{\eta} + \left(-\gamma + \sum_{k=1}^{2n}\frac{1}{k}\right) + \sum_{m=2}^{\infty}(-1)^m\eta^{m-1}\left[-\sum_{k=1}^{2n}\frac{1}{k^m} + \xi(m)\right.$$
$$\left. -\left(\frac{1}{2^m} + \frac{1}{(-2)^m}\right)\xi(m)\right] = -\ln(\tfrac{1}{4}\rho) \tag{6.11a}$$

[15] BMP, Vol. 1, p. 5, Eq. (15).
[16] BMP, Vol. 1, p. 45, Eq. (2). $\xi(m)$ is the Riemann zeta function.
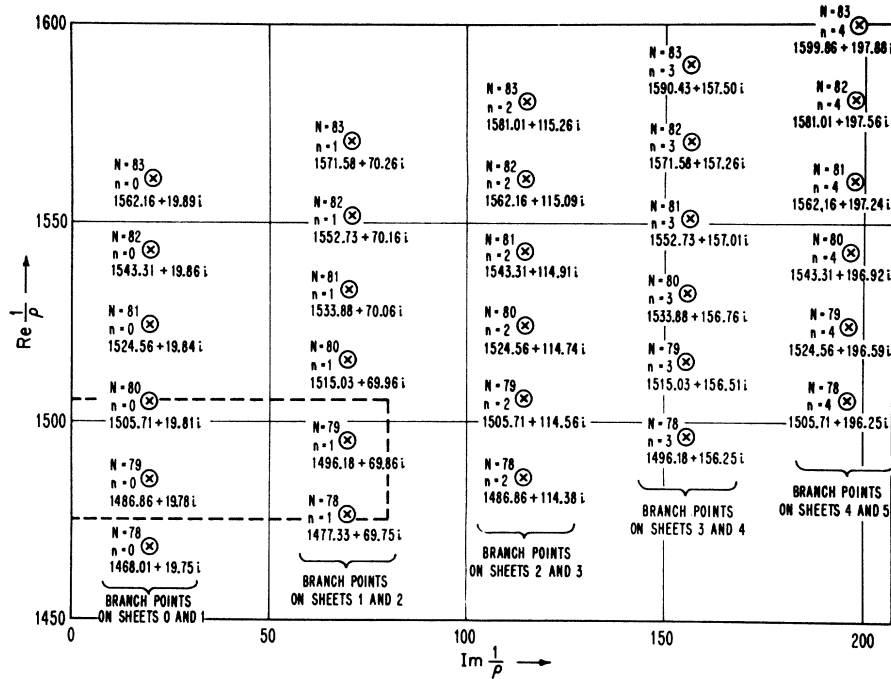[17] BMP, Vol. 1, p. 45, Eq. (5).

FIG. 2. A portion of the $1/\rho$ plane on which are plotted the even-parity branch points. The branch points are labeled by the integers n ranging from 0 through 4 and N ranging from 78 to 83. Next to each branch point are its coordinates correct to the nearest hundredth. The region of the graph surrounded by the dashed line is enlarged in Fig. 4 and will be discussed in connection with level crossing.

Branch points plotted in the $1/\rho$ plane (vertical axis $\mathrm{Re}\,\tfrac{1}{\rho}$ from 1450 to 1600; horizontal axis $\mathrm{Im}\,\tfrac{1}{\rho}$ from 0 to 200):

BRANCH POINTS ON SHEETS 0 AND 1:
- $N=83$, $n=0$: $1562.16+19.89i$
- $N=82$, $n=0$: $1543.31+19.86i$
- $N=81$, $n=0$: $1524.56+19.84i$
- $N=80$, $n=0$: $1505.71+19.81i$
- $N=79$, $n=0$: $1486.86+19.78i$
- $N=78$, $n=0$: $1468.01+19.75i$

BRANCH POINTS ON SHEETS 1 AND 2:
- $N=83$, $n=1$: $1571.58+70.26i$
- $N=82$, $n=1$: $1552.73+70.16i$
- $N=81$, $n=1$: $1533.88+70.06i$
- $N=80$, $n=1$: $1515.03+69.96i$
- $N=79$, $n=1$: $1496.18+69.86i$
- $N=78$, $n=1$: $1477.33+69.75i$

BRANCH POINTS ON SHEETS 2 AND 3:
- $N=83$, $n=2$: $1581.01+115.26i$
- $N=82$, $n=2$: $1562.16+115.09i$
- $N=81$, $n=2$: $1543.31+114.91i$
- $N=80$, $n=2$: $1524.56+114.74i$
- $N=79$, $n=2$: $1505.71+114.56i$
- $N=78$, $n=2$: $1486.86+114.38i$

BRANCH POINTS ON SHEETS 3 AND 4:
- $N=83$, $n=3$: $1590.43+157.50i$
- $N=82$, $n=3$: $1571.58+157.26i$
- $N=81$, $n=3$: $1552.73+157.01i$
- $N=80$, $n=3$: $1533.88+156.76i$
- $N=79$, $n=3$: $1515.03+156.51i$
- $N=78$, $n=3$: $1496.18+156.25i$

BRANCH POINTS ON SHEETS 4 AND 5:
- $N=83$, $n=4$: $1599.86+197.88i$
- $N=82$, $n=4$: $1581.01+197.56i$
- $N=81$, $n=4$: $1562.16+197.24i$
- $N=80$, $n=4$: $1543.31+196.92i$
- $N=79$, $n=4$: $1524.56+196.59i$
- $N=78$, $n=4$: $1505.71+196.25i$

and

$$\frac{1}{\eta}+\left(-\gamma+\sum_{k=1}^{2n+1}\frac{1}{k}\right)+\sum_{m=2}^{\infty}(-1)^m\eta^{m-1}\left[-\sum_{k=1}^{2n+1}\frac{1}{k^m}+\xi(m)\right.$$

$$\left.-\left(\frac{1}{2^m}+\frac{1}{(-2)^m}\right)\xi(m)\right]=-\ln(\tfrac{1}{4}\rho). \quad (6.11b)$$

Equations (6.9) and (6.11) are now in a form amenable to approximate simultaneous solution. The expansions in Eqs. (6.9) and (6.11) are power series in η and are most susceptible to techniques of approximation if $|\eta|\ll1$. η is indeed small as will be seen. N is a large integer.

The simultaneous solution consists of using Eqs. (6.9) and (6.11) alternatively to provide successively more accurate approximations to $1/\rho$ and $1/\eta$. First, we use Eq. (6.9). To zeroth order in η, the locations of the singularities in the analytic continuation $E(\lambda)$ are approximately

$$1/\rho=6\pi N \quad (6.12a)$$

and

$$1/\rho=6\pi(n+1). \quad (6.12b)$$

Next we use Eqs. (6.12) and (6.11) to find $1/\eta$ to zeroth order in η:

$$\frac{1}{\eta}=\ln(24\pi N)+\gamma-\sum_{k=1}^{2n}\frac{1}{k} \quad (6.13a)$$

and

$$\frac{1}{\eta}=\ln[24\pi(N+1)]+\gamma-\sum_{k=1}^{2n+1}\frac{1}{k}. \quad (6.13b)$$

Remembering that N is large, we see that Eq. (6.13) verifies the earlier assumption that $|\eta|$ is small. We use Eqs. (6.13) and (6.9) and iterate once more to find the locations of the singularities of $E(\lambda)$ to first order in η:

$$1/\rho=6\pi N+3\pi n-3\pi/4-3i[\ln(2n)!+\tfrac12\ln(\pi/2)$$
$$-\ln\ln N-(2n+\tfrac12)\ln(24\pi N)-1] \quad (6.14a)$$

and

$$1/\rho=6\pi(N+1)+3\pi n+3\pi/4-3i\{\ln(2n+1)!$$
$$+\tfrac12\ln(\pi/2)-\ln\ln N-(2n+\tfrac32)$$
$$\times\ln[24\pi(N+1)]-1\}. \quad (6.14b)$$

Equation (6.14) is the equation we have sought. It lists the coordinates of the branch points of $E(\lambda)$ parametrized by two integers N (large) and n (small).

Before discussing this equation, it is appropriate to make some observations here on the structure of Eqs. (6.9) and (6.11), the simultaneous equations that were used to derive Eq. (6.14). We note that Eq. (6.11) is the derivative of Eq. (6.9) with respect to η. This is true because Eq. (6.3) is the logarithmic derivative of Eq. (6.1) with respect to E. However, the significance of this relationship is not obvious.

An explanation for this relationship comes from a broader interpretation of Eqs. (4.35) than we have chosen to use. We might have assumed that Eqs. (4.35) were more than just equations relating E and λ for small λ. We might have treated them as approximate (to zeroth order in λ) analytic continuations of E as a function of λ. Based on this assumption, the condition for locating those points in the λ plane where the energy
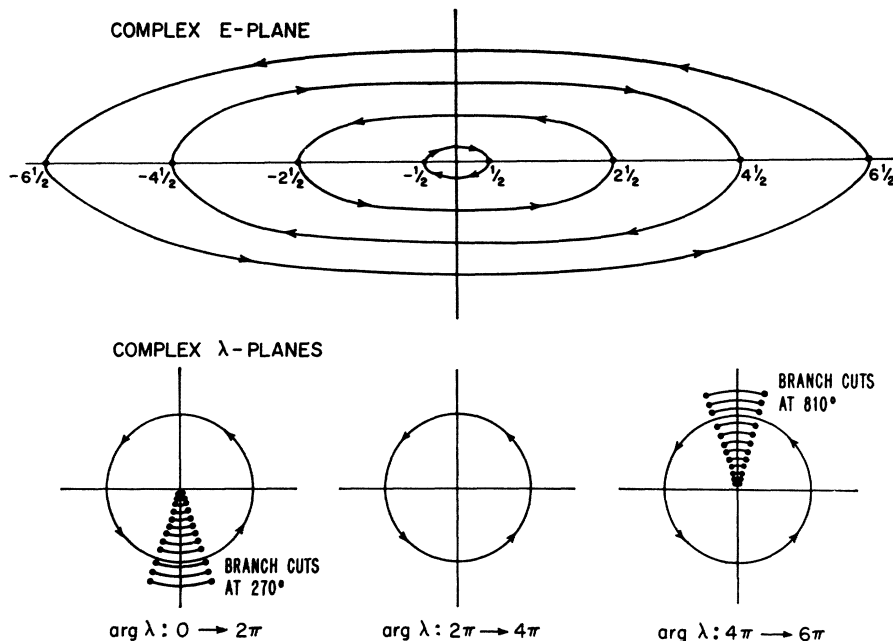
COMPLEX E-PLANE

COMPLEX λ-PLANES

FIG. 3. A rough picture of a tour of the λ plane with the associated image of $E(\lambda)$ in the E plane. $|\lambda|$ is held fixed while argλ ranges from 0 to 6π. The λ plane is drawn as three planes to show the full rotation of argλ. The branch points and arc-shaped branch lines are indicated schematically. The graph gives the paths of the even-parity energy levels only. The odd-parity levels behave similarly.

BRANCH CUTS AT 810°

BRANCH CUTS AT 270°

arg λ: 0 → 2π   arg λ: 2π → 4π   arg λ: 4π → 6π

is twofold degenerate would be that the derivative of Eq. (6.9) with respect to E (or η) must be a valid equation. Because it gives the correct answer, this argument would have constituted a "derivation" of Eq. (6.11) and would have been a short cut past Appendix G.

We did not use the above argument on grounds of rigor. It is not clear what is meant by an "approximate zeroth-order analytic continuation." It is difficult to understand how one could approximate an exact concept like analyticity by zeroth-order techniques. The laborious method of getting Eq. (6.11) by deriving and evaluating $\int_C \Phi^2(x)dx$ in Sec. III and Appendix G was presented in this paper to avoid these mathematical imprecisions.

Having made this point we return to analyze Eq. (6.14). We note that as the integer N takes on a sequence of values approaching ∞, the associated sequence of branch points in the λ plane given by Eq. (6.14) begins at a finite distance from the origin and has a limit point at the origin. (Remember that $\rho = \lambda e^{-3\pi i/2}$.) That this sequence of branch points has a limit point at the origin explains the divergence of the perturbation series discussed earlier in Sec. II. Note that the origin in the λ plane is not an isolated singularity of $E(\lambda)$.

It is useful to plot the results of Eq. (6.14) on a graph. Figure 2 shows a portion of the $1/\rho$ plane on which are plotted the even-parity branch points labeled by the integer n ranging from 0 through 4 and N ranging from 78 to 83. Next to each branch point are its coordinates correct to two decimal places. The region of the graph surrounded by the dashed line is blown up in Fig. 4 and will be discussed in detail in Part C of this section in connection with level crossing.

It is clear from Fig. 2 that the branch points lie in a sequence of sequences. Each sequence of branch points is labeled by n and each sequence approaches the origin. A glance at Fig. 4 shows that the first $(n=0)$ sequence of points lies at an angle of about $\frac{3}{4}°$ less than 270° in the λ plane. The next $(n=1)$ sequence lies approximately $2\frac{1}{2}°$ less than 270°. Each successive sequence is rotated by a small angle toward the real axis in the λ plane.

However, we suspect that as n increases, these sequences bunch up before they reach 180° and that no branch points have a complex argument of less than 180°. If there were such branch points then, by the argument of Sec. V, the resolvent of the Hamiltonian would have poles in the cut λ plane. Jaffe[2] proved that this is not so. Unfortunately, Eq. (6.14) only holds for small n so this bunching phenomenon cannot be illustrated graphically.[18]

B. Paths in E Plane

Having found the branch points of $E(\lambda)$, we can give a qualitative picture of the complex function $E(\lambda)$. We will do this by tracing the paths of the energy levels in the complex E plane as λ moves about the complex λ plane.

We begin our analysis by observing that both differential equations [Eqs. (4.1) and (4.9)] are real in

[18] In Sec. VI C, it will be shown that the WKB solution [Eq. (6.1)] is valid in two semidisk-shaped regions of the λ plane bounded by argλ=270°±90° and argλ=810°±90°. In the rest of the λ plane, the WKB solution is superseded by Eq. (4.8). Since the existence of branch points is a phenomenon associated only with Eq. (6.1), branch points must lie throughout the region in which Eq. (6.1) holds. Therefore, we expect that the bunching phenomenon occurs at the boundaries of the region; that is, at argλ = 180°, 360°, 720°, and 900°.

their respective variables. From this arise some symmetry properties of $E(\lambda)$ which are

$$E(\lambda)=E^*(\lambda^*)=-E^*(e^{3\pi i}\lambda^*)=-E(e^{3\pi i}\lambda). \quad (6.15)$$

We also note that since the Hamiltonian [Eq. (1.3)] is Hermitian and positive definite, the energy levels lie along the positive real axis in the energy plane when λ is positive real. Similarly, when $\arg\lambda=270°$, Eq. (4.9) indicates that the energy levels are pure imaginary. At $\arg\lambda=270°$, the energy levels lie on both the positive and negative imaginary axes.

Equation (4.8) indicates that for fixed $|\lambda|$ the energy levels lie near the real axis in the energy plane as $\arg\lambda$ increases from 0 until nearly 270°. However, for $\arg\lambda$ in the neighborhood of 270° the full energy spectrum moves rapidly toward the imaginary axis.

Combining the symmetry properties [Eq. (6.1)] with the results of the previous two paragraphs enables us to predict the paths of the energy levels in the complex E plane when $|\lambda|$ is held fixed and $\arg\lambda$ is varied. (These paths are given in Fig. 3.) We predict that:

(i) When $\arg\lambda=0$, the energy spectrum lies along the positive real axis.

(ii) As $\arg\lambda$ increases toward $\frac{1}{4}(6\pi)$, each energy level traces out a path in the complex E plane which approaches the imaginary axis. The energy levels lie along the imaginary axis at $\arg\lambda=\frac{1}{4}(6\pi)$.

(iii) At $\arg\lambda=\frac{1}{2}(6\pi)$, the energy levels lie on the negative real axis at points equal to the negative of their original values for $\arg\lambda=0$.

(iv) As $\arg\lambda$ increases from $\frac{1}{2}(6\pi)$ to 6π, each energy level traces a path reflectionally symmetric about the origin to the path described above. At $\arg\lambda=6\pi$ the energy levels return to the values on the real axis that they had for $\arg\lambda=0$.

Thus, as λ goes in a circle three times about the origin in the λ plane, starting at the real axis, each energy level in the E plane traces a closed path starting and ending on the positive real axis. Moreover, it will be shown in Part C of this section that the paths in the complex E plane are concentric and that the directions of successive concentric paths alternate between clockwise and counterclockwise.

Because the energy levels return to their original values when $\arg\lambda$ is increased by 6π, in addition to the branch-point singularities discussed in Part A of this section there is also a $\lambda^{1/3}$ singularity at the origin. However, the divergence of perturbation theory discussed in Sec. II is in no way related to this singularity. If it were, we could then expand $E(\lambda)$ in powers of $\lambda^{1/3}$ and get a convergent power series. But there is no convergent power-series representation of $E(\lambda)$ about the origin in any fractional power of λ. Perturbation theory diverges because of the sequences of branch points discussed in Part A of this section.

How do these branch points affect the curves in the E plane in Fig. 3? Surprisingly, the answer to this

question is "*not at all.*" To understand why this is we argue as follows:

(i) As proved in Sec. III, each of these singularities is a square-root type. (In the neighborhood of each branch point, there is a double-sheeted Riemann surface.) Level crossing (twofold degeneracy) must occur at each branch point. A branch line is connected to each singularity.

(ii) The symmetry properties listed in Eq. (6.15) imply that there is another set of branch points symmetrically reflected about 270° in the λ plane. Moreover, all these singularities (those in Fig. 2 and those reflected through 270°) also must occur at $-270°$ (which is the same as 810° because of the cube-root singularity at the origin).

(iii) The branch lines join the branch points on either side of 270° and on either side of 810° pairwise; that is, each point is joined to its reflected image. These branch cuts are shaped like circular arcs and are very short because the branch points lie a short distance from either side of 270° or 810°. The cuts form two sequences of concentric arcs with each sequence of arcs approaching the origin. These cuts are schematically displayed on Fig. 3.

(iv) In the circular tour of the λ plane shown on Fig. 3 it is clear that none of the branch cuts was crossed because $|\lambda|$ was held fixed.

This reasoning explains why the branch points could not affect the curves in the E plane in Fig. 3. In addition, it shows that the presence of the branch points can never be detected as long as $|\lambda|$ is held fixed.

Therefore, to exhibit the delicate intricacy of this theory caused by the array of cuts in Fig. 3, we must make a new tour of the λ plane in which we cross the branch cuts. We still increase $\arg\lambda$ from 0 to 6π. However, when $\arg\lambda$ is near 270° (or 810°) we vary $|\lambda|$ so that the path in the λ plane crosses a branch line. If we follow an energy level as it traces a path in the complex E plane, we find that it returns to the positive real axis when $\arg\lambda=6\pi$ but as a different energy level from the original. This is what is meant by level crossing.

A complete description of level crossing is given in Part C of this section. Nevertheless, it should now be clear that the energy levels are completely interrelated by the structure of the branch cuts. That is, one can get to any given energy level from any other energy level by continuing around the appropriate branch points.

As a corollary of this, once one knows the ground-state energy of the anharmonic oscillator, one knows all the energy levels by analytic continuation. Or, in other words, *the physical energy levels of the anharmonic oscillator for a given positive real λ are the positive real values of $E(\lambda)$ on each of the infinite number of branches of a Riemann surface. Each energy level corresponds to a sheet of this Riemann surface.* This is the major result of our paper.

FIG. 4. An enlargement of a small portion of the 1/ρ plane of Fig. 2. The $(N=78, n=1)$, $(N=79, n=0)$, $(N=79, n=1)$, and $(N=78, n=1)$ branch points are precisely located. Four short circular arcs of unequal radii are drawn and the angular rotation along each arc is given in degrees. The arcs are indicated by a solid line, dashed line, dash-dotted line, and dotted line. The radii of these arcs to the nearest hundredth are 1496.50, 1490.50, 1487.50, and 1484.50, respectively. The images of these arcs in the E plane are plotted on Fig. 5 in connection with level crossing.
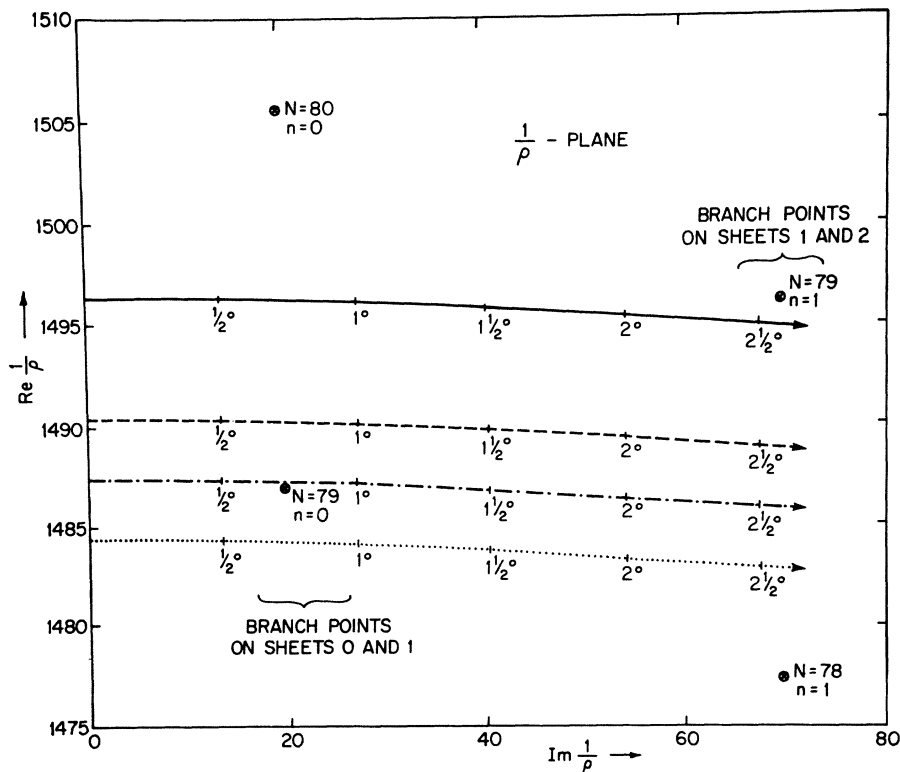
C. Level Crossing

We have shown that level crossing takes place at the branch points in the λ plane and we know the positions of these branch points. But the details of level crossing are not yet fully explained. In particular, in this part of Sec. VI we will answer these questions: (a) Which levels cross at which branch points? (b) What does level crossing look like graphically?

To give a precise answer to these questions, we carry out an intensive program of numerical calculation which enables us to construct Figs. 4 and 5. Figures 4 and 5 will give a beautiful pictorial answer to the questions we have posed. The numerical calculation involves the following procedure:

(i) We take a sequence of circular paths of varying radii in the 1/ρ plane. (This is equivalent to and easier to handle numerically than a sequence of circles in the λ plane.) The image of each of these circles in the E plane is a set of energy-level curves like those crudely drawn in Fig. 3. As in Fig. 3, we will consider the even-parity case only. (The odd-parity case is qualitatively similar.)

(ii) By symmetry [see Eq. (6.15) and the accompanying discussion] we need only to vary argλ from 0° to 270°. Moreover, until argλ is very nearly 270°, the energy levels stay extremely close to the values given in Eq. (4.8a). Therefore, we only need to consider the portions of the energy-level curves for λ near 270° (that is, where 1/ρ is approximately real).

(iii) We choose the sequence of radii in the 1/ρ plane so that a branch point is crossed. We then use Eq. (6.1a) to plot points accurately in the E plane and expect to observe the process of level crossing. We choose four values for the radii of the curves in the 1/ρ plane. To the nearest hundredth, these values of $|1/ρ|$ are 1496.50, 1490.50, 1487.50, and 1484.50. These curves are drawn on Fig. 4. (Figure 4 is an enlarged version of a part of Fig. 2. That portion which is enlarged is indicated on Fig. 2 by a dashed line.) The branch point that is crossed is the one labeled $N=79$, $n=0$.

(iv) We then choose points along the curves in Fig. 4 and solve the transcendental equation [Eq. (6.1)] numerically for complex E to the nearest hundredth. To solve Eq. (6.1a) numerically we take the logarithm of both sides. This gives

$$\ln\Gamma(\tfrac{1}{4}+\tfrac{1}{2}E)-\ln\Gamma(\tfrac{1}{4}-\tfrac{1}{2}E)$$

$$=\frac{i}{3\rho}+\frac{5\pi i}{4}+E\ln\frac{2}{\rho}+2\pi iM. \quad (6.16)$$

M is an integer referring to the many-valued logarithmic function. M occurs for the same reason that N did in Eq. (6.7).

(v) We choose the branch line for the logarithmic function in Eq. (6.16) to lie along the negative real axis. We then break up Eq. (6.16) into its real and imaginary parts and, given 1/ρ, solve the resulting
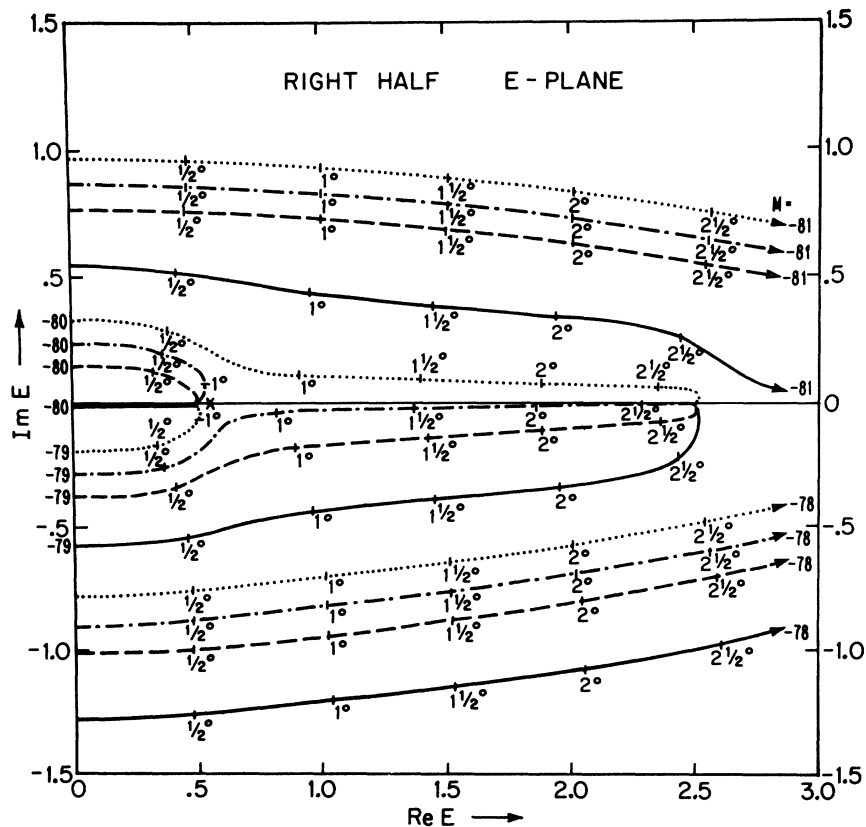
FIG. 5. The complex E plane, showing to the nearest hundredth the images of the circular arcs in the $1/\rho$ plane of Fig. 4. These curves exhibit level crossing. The precise point where this level crossing occurs is marked with an **X**. **X** is the image of the branch point ($N=79$, $n=0$). The energy-level curves shown correspond with the four lowest energy levels. The curves are labeled by their M values [see Eq. (6.16)] and are represented by dotted, dot-dashed, dashed, and solid lines to correspond with the values of $|1/\rho|$ on Fig. 4 (1484.50, 1487.50, 1490.50, and 1496.50). The numbers in degrees along each curve indicate the rotation in the $1/\rho$ plane of the preimage points along the curves on Fig. 4.

pair of simultaneous transcendental equations for E. The solution is a painstaking trial-and-error process involving tables of $\ln\Gamma(z)$ functions. Fortunately, this mammoth task is tractable because $\arg(1/\rho)$ is small, ranging from 0 to approximately $3°$ (see Fig. 4). Several hundred values for E have been plotted on Fig. 5 and the energy-level curves have been drawn and labeled by their M values. We have plotted the energy-level curves connected to the four lowest energy levels.

This completes the description of the construction of Figs. 4 and 5. We list below our observations and conclusions with regard to these graphs.

As $|1/\rho|$ gets smaller, we observe that the points where the energy-level curves meet the imaginary axis in the E plane move upward. {This fact can be proved from the differential equation [Eq. (4.9)] independently of the numerical calculations involved in the graphing of Fig. 5.} Therefore, as $|1/\rho|$ decreases, either we will find that (a) level crossing occurs (that is, the curves associated with a given M value become associated with different energy values along the real E axis) or else that (b) the curves all remain attached to the same energy values on the real E axis and stretch higher and higher up the imaginary axis. The enormous distortion of the curves in the latter possibility (b) makes the former (a) a good probability.

Level crossing is indeed found on inspection of Fig. 5. (For each value of M the curves on Fig. 5 are represented in order of decreasing $|1/\rho|$ by solid lines, dashed lines, dash-dotted lines, and dotted lines.) We observe the following example of level crossing.

The solid $M=-79$ line is connected to $E=2\frac{1}{2}$ along the real axis. There is just a hint of inflection as this curve passes below $E=\frac{1}{2}$. Its companion, the solid $M=-80$ line, goes directly to $E=\frac{1}{2}$ and the dash-dotted line inflects strongly. Meanwhile, the companion $M=-80$ lines belly increasingly outward above $E=\frac{1}{2}$ to meet the inflecting $M=-79$ lines. As the curves in the $1/\rho$ plane pass through the $N=79$, $n=0$ branch point, the energy levels flip and the dotted $M=-79$ line is suddenly and discontinuously connected to $E=\frac{1}{2}$ and the companion $M=-80$ line to $E=2\frac{1}{2}$. *This is a precise pictorial description of level crossing.*

It is interesting to determine where the curves connecting $F=\frac{1}{2}$ and $E=2\frac{1}{2}$ cross. To determine this crossing point we have calculated the image of the branch point $N=79$, $n=0$ in the E plane. The crossing point is labeled on Fig. 5 by an **X**.

In addition to the above level crossing we also observe an incipient level crossing at $E=2\frac{1}{2}$. As we look at the lines in the opposite order (dotted, dot-dashed, dashed, and solid), we see on Fig. 4 that a level crossing is about to take place at the $N=79$, $n=1$

branch point. The solid lines $M=-81$ and $M=-79$ are ready to cross near $E=2\frac{1}{2}$.

As $|\lambda|$ increases and the circle in the λ plane passes through the appropriate branch points, each pair of adjacent levels flips repeatedly. *Only adjacent levels can cross.* For example, the zeroth and first energy levels cross at $n=0$ branch points, the $n=1$ and $n=2$ energy levels cross at $n=1$ branch points, and so on. In general, *the nth sequence of branch points is common to and lies only on the nth and $(n+1)$st sheets of the Riemann surface of $E(\lambda)$.* (Remember that the nth sheet is the sheet which contains the nth energy level for real positive λ.) This is equivalent to saying that *the nth and $(n+1)$st energy levels can only cross at the nth sequence of branch points.*

Figure 5 evokes an additional, unexpected, and most welcome observation. Recall that near $\lambda=270°$ the WKB equation [Eq. (6.1a)] describes the paths of the energy levels in the E plane. Near $\text{arg}\lambda=0$, Eq. (4.8a) describes these paths. Therefore, at some value of $\text{arg}\lambda$ between $270°$ and $0°$, Eq. (6.1a) is no longer accurate and is superseded by Eq. (4.8a). The angle at which this changeover occurs defines the angular opening about $270°$ (and $810°$) in which the WKB solution is valid. The numerical investigations used to plot Fig. 5 give answers to two important questions: (a) At what angle does the changeover occur? (b) How accurate is the WKB result?

To answer these questions, we notice that the curves on Fig. 5 all approach the values predicted by Eq. (4.8a) which are $E=\frac{1}{2}$, $2\frac{1}{2}$, $4\frac{1}{2}$, $\cdots$. However, at some angle in the $1/\rho$ plane the WKB result [Eq. (6.1a)] no longer directs the energy-level curves toward these values. At that angle the curves begin to veer away. Therefore, the angle at which the curves are closest to the points $E=\frac{1}{2}$, $2\frac{1}{2}$, $4\frac{1}{2}$, $\cdots$ is the answer to question (a). Furthermore, the *distance* of closest approach of the WKB curves to these points is a useful measure of how accurate the WKB solution is and will answer question (b). The WKB result is accurate if the distance of closest approach is small.

It is easy to calculate the changeover angle and the distance of closest approach. We expand $\ln\Gamma(\frac{1}{4}-\frac{1}{2}E)$ in a Taylor series[16] about $E=\frac{1}{2}$, $2\frac{1}{2}$, $4\frac{1}{2}$, $\cdots$, and insert the series into Eq. (6.16). We determine from the resulting equation that $\text{arg}(1/\rho)=90°$ is the condition for closest approach. That is, the WKB result applies in an angular opening of $90°$ on either side of $\text{arg}\lambda=270°$ (and $810°$). This answers question (a). This angular opening is much wider than originally anticipated and shows that the WKB solution is valid in a very large region of the λ plane.

Furthermore, the changeover angle at $\text{arg}\lambda=180°$ ties in beautifully with three earlier results of this paper, First, Fig. 1(c) in Sec. IV shows that it is exactly at $\text{arg}\lambda=180°$ that the WKB turning point enters the sector in which the general boundary con-

dition [Eq. (3.4)] applies. This is just the point at which we would expect Eq. (6.1a), the WKB equation, to become valid. Second, a changeover angle of $180°$ indicates that the bunching phenomenon discussed in Part A of Sec. VI takes place at $180°$.[18] Third, when combined with the arguments of Sec. V, a changeover angle of $180°$ implies that the poles of the resolvent occur when $\text{arg}\lambda$ is larger than $180°$. This is consistent with Jaffe's findings.[2]

A short numerical calculation reveals that the distance of closest approach to $E=\frac{1}{2}$ is the amazingly small number $\frac{1}{3}\times10^{-153}$. This distance is much smaller than originally anticipated. It is gratifying to observe that, in answer to question (b), the WKB solution is extremely accurate.

ACKNOWLEDGMENTS

APPENDIX A

In this appendix, we use field theory to derive the coordinate representation given by Eqs. (1.1) and (1.2) which are

$$(-d^2/dx^2+\tfrac{1}{4}x^2+\tfrac{1}{4}\lambda x^4)\Phi(x)=E(\lambda)\Phi(x) \qquad \text{(A1)}$$

and

$$\lim_{x\to\pm\infty}\Phi(x)=0. \qquad \text{(A2)}$$

A quick derivation follows from substituting

$$\varphi=2^{-1/2}x \quad \text{and} \quad \dot{\varphi}=-i2^{1/2}d/dx \qquad \text{(A3)}$$

into the Hamiltonian H [Eq. (1.3)] which is

$$H=\tfrac{1}{2}\dot{\varphi}^2+\tfrac{1}{2}m^2\varphi^2+\lambda\varphi^4. \qquad \text{(A4)}$$

We choose $m=1$ without loss of generality. Then the wave function $\Phi(x)$ satisfies the differential equation [Eq. (A1)]. Equation (A2) results from the requirement that $\Phi(x)$ be normalizable.

A more rigorous derivation follows from the assumption that in Fock space the energy eigenstates of H are normalizable.

In the interaction picture, the representation of the field φ in terms of creation and annihilation operators on Fock space is

$$\varphi=[1/(2m)^{1/2}](ae^{-imt}+a^\dagger e^{imt}), \qquad \text{(A5a)}$$

$$\dot{\varphi}=(\tfrac{1}{2}m)^{1/2}(-iae^{-imt}+ia^\dagger e^{imt}), \qquad \text{(A5b)}$$

$$[a,a^\dagger]=1. \qquad \text{(A5c)}$$

In terms of the creation and annihilation operators, the Hamiltonian is

$$H=m(a^\dagger a+\tfrac{1}{2})+(g/4m^2)(a+a^\dagger)^4. \qquad \text{(A6)}$$

Let $|E\rangle$ be an eigenstate of H of energy E. Then

$$H|E\rangle = E|E\rangle. \tag{A7}$$

The Fock representation consists of the states

$$|n\rangle = [1/\sqrt{(n!)}](a^\dagger)^n|0\rangle, \quad n = 0, 1, 2, \cdots \tag{A8a}$$

where

$$\langle n|m\rangle = \delta_{nm}. \tag{A8b}$$

Assuming that $\{|n\rangle\}$ are a complete set of states,

$$|E\rangle = \sum_{n=0}^{\infty} a_n|n\rangle\sqrt{(n!)}. \tag{A9}$$

Equations (A6)–(A9) can be combined to give a difference equation that the $\{a_n\}$ satisfy:

$$Ea_n = m(n+\tfrac{1}{2})a_n + (g/4m^2)[a_{n-4} + 4(n-2)a_{n-2}$$
$$+ 6n(n-1)a_n + 4n(n+1)(n+2)a_{n+2}$$
$$+ (n+1)(n+2)(n+3)(n+4)a_{n+4}]. \tag{A10}$$

Furthermore, since $|E\rangle$ is assumed normalizable,

$$\sum_{n=0}^{\infty} |a_n|^2 n! < \infty. \tag{A11}$$

From Eq. (A11) it follows that as $n \to \infty$, $|a_n| \to 0$ faster than $1/\sqrt{(n!)}$. Thus, if we define the generating function $f(z)$ by

$$f(z) = \sum_{n=0}^{\infty} a_n z^n, \tag{A12}$$

then $f(z)$ is entire.

The difference equation [Eq. (A10)] becomes a differential equation satisfied by $f(z)$:

$$Ef(z) = \frac{g}{4m^2}\left(z + \frac{d}{dz}\right)^4 f(z) + mz\frac{d}{dz}f(z) + \tfrac{1}{2}mf(z). \tag{A13}$$

The differential equation [Eq. (A13)] and the side condition that $f(z)$ is entire embody the assumption that $|E\rangle$ is an eigenstate of H of finite norm and that $\{|n\rangle\}$ are a complete set of states.

Now let

$$f(z) = e^{-z^2/2}h(z). \tag{A14}$$

Then,

$$Eh(z) = (g/4m^2)h''''(z)$$
$$+ m[zh'(z) - z^2h(z)] + \tfrac{1}{2}mh(z). \tag{A15}$$

Next we show that $h(z)$ must go to 0 rapidly along the imaginary axis. To do this, we apply the Cauchy formula to Eq. (A12):

$$a_n = \frac{1}{2\pi i}\oint \frac{f(z)}{z^{n+1}}dz = \frac{1}{2\pi i}\oint \frac{e^{-z^2/2}g(z)}{z^{n+1}}. \tag{A16}$$

Suppose that $g(z)$ did not go to 0 along the imaginary axis. In fact, suppose for simplicity that $g(z)$ were

constant. Then, since the major contribution to this integral would come from the region where the path of integration crosses the imaginary axis, we calculate (using the method of steepest descent) that $a_n \sim A/\sqrt{n}$ for large n. This contradicts Eq. (A11) and the entirety of $f(z)$. Hence, $h(z)$ must go to 0 along the imaginary axis.

To see how fast $h(z) \to 0$, we consider the differential equation for $h(z)$ [Eq. (A15)]. By systematically investigating pairs of terms, we find that the dominant behavior at large z is given by

$$(g/4m^2)h''''(z) - mz^2h(z) = 0. \tag{A17}$$

Thus,

$$h(z) \sim \exp[C\tfrac{2}{3}(4m^2/g)^{1/4}z^{3/2}], \tag{A18}$$

where $C = 1$, -1, i, $-i$. Since there are four solutions to the fourth-order differential equation [Eq. (A17)], we have them all. Combining Eq. (A18) with our knowledge that $h(z)$ goes to 0 along the imaginary axis, we learn that $h(z)$ goes to 0 along the imaginary axis extremely rapidly. Hence, $h(z)$ may be Fourier-transformed along the imaginary axis. We thus define (for real x)

$$h(z) = \int_{-\infty}^{\infty} H(x)e^{zx}dx. \tag{A19}$$

Fourier-transforming Eq. (A15) according to Eq. (A19) gives

$$mH''(x) + mxH'(x) + (E + \tfrac{1}{2}m)H(x)$$
$$- (g/4m^2)x^4H(x) = 0. \tag{A20}$$

Finally, we let

$$H(x) = e^{-x^2/4}\Phi(x). \tag{A21}$$

This substitution [Eq. (A21)] simplifies (A20) to

$$m\Phi''(x) + E\Phi(x) - \tfrac{1}{4}mx^2\Phi(x) - (g/4m^2)x^4\Phi(x) = 0. \tag{A22}$$

Equation (A22) implies that the dominant behavior of Φ for large x is $e^{|x|^3}$ or $e^{-|x|^3}$. The former is not possible because the inverse transform would not exist and $h(z)$ would be undefined. Hence, $\Phi(x) \to 0$ as $|x| \to \infty$.

We set $m = 1$ as we did earlier in this appendix and Eq. (A22) becomes

$$-\Phi''(x) + \tfrac{1}{4}x^2\Phi(x) + \tfrac{1}{4}\lambda x^4\Phi(x) = E\Phi(x), \tag{A23}$$

and

$$\lim_{|x| \to \infty} \Phi(x) = 0. \tag{A24}$$

Equations (A23) and (A24) are precisely Eqs. (A1) and (A2). We have thus rigorously derived the coordinate representation and the boundary condition satisfied by the wave function Φ.

This connection between field theory and the wave function in coordinate space will be used in Sec. II and Appendices B and C.

APPENDIX B

In this appendix, we use Feynman rules to calculate A_1, A_2, and A_3. These are the first three terms beyond the constant zero-point energy term in the perturbation series for the ground-state energy [Eq. (2.1)]. The Feynman rules for the anharmonic oscillator considered as a field theory are

$$(E^2-m^2+i\epsilon)^{-1} \quad \text{for a propagator}, \quad \text{(B1a)}$$

$$24\lambda \quad \text{for a vertex}, \quad \text{(B1b)}$$

$$i(2\pi)^{-1}\int_{-\infty}^{\infty} dE \quad \text{for a loop integration}. \quad \text{(B1c)}$$

The symmetry numbers are the same as in the (3+1)-dimensional theory.[19]

The nth term in the perturbation series for the ground-state energy is the sum of all connected n-vertex Feynman diagrams with no external legs. (Each diagram is of course multiplied by its appropriate symmetry number.) Figure 6 shows all such diagrams of order $n=1$, 2, and 3 with their symmetry numbers.[20]

We find the contribution of each of the diagrams by applying the Feynman rules [Eq. (B1)] and by evaluating the resulting simple contour integrals. This calculation yields

$$
\begin{aligned}
(1a) &= (24)\tfrac{1}{4}(\lambda/m^3)m, \\
(2a) &= (24)^2(-1/16)(\lambda/m^3)^2 m, \\
(2b) &= (24)^2(-1/32)(\lambda/m^3)^2 m, \\
(3a) &= (24)^3(3/128)(\lambda/m^3)^3 m, \quad \text{(B2)} \\
(3b) &= (24)^3(5/512)(\lambda/m^3)^3 m, \\
(3c) &= (24)^3(3/512)(\lambda/m^3)^3 m, \\
(3d) &= (24)^3(1/64)(\lambda/m^3)^3 m.
\end{aligned}
$$

Next, we combine the symmetry numbers listed on Fig. 6 with Eq. (B2) and find that[21]

$$A_1 = (24/4)\times\tfrac{1}{8} = \tfrac{3}{4}, \quad \text{(B3a)}$$

$$A_2 = -\frac{(24)^2}{16\times16}-\frac{(24)^2}{32\times48} = -\frac{21}{8}, \quad \text{(B3b)}$$

---

[19] T. T. Wu, Phys. Rev. **125**, 1436 (1962).

[20] The interaction we are discussing is not Wick-ordered. If it were Wick-ordered, only diagrams (2b) and (3c) would contribute to the ground-state-energy perturbation series. All other diagrams would be excluded because they have at least one line emerging from and returning to the same vertex.

[21] In the definition of the ground-state-energy perturbation series [Eq. (2.1)], which is

$$E_0(\lambda) = \tfrac{1}{2}m + \sum_{n=1}^{\infty} (\lambda/m^3)^n m A_n,$$

the factors of m and $(\lambda/m^3)^n$ have been isolated from the A_n.
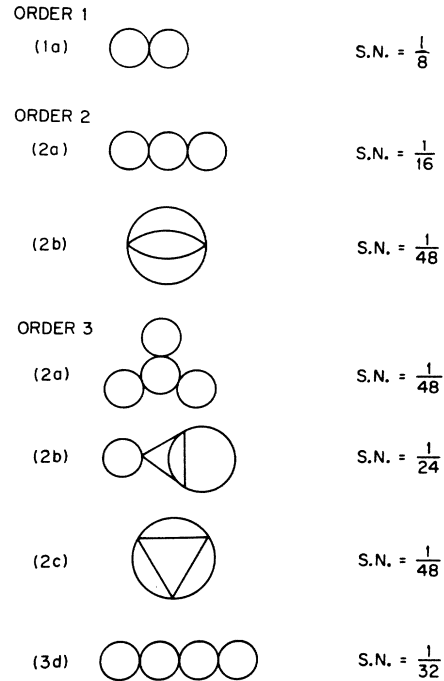

FIG. 6. All connected Feynman diagrams of order $n=1$, 2, and 3 with no external legs. To the right of each diagram is its symmetry number (S.N.).

$$A_3 = =\frac{(24)^3\times3}{128\times48}+\frac{(24)^3\times5}{512\times24}+\frac{(24)^3\times3}{512\times48}$$

$$+\frac{(24)^3}{64\times32}=\frac{333}{16}. \quad \text{(B3c)}$$

The results in Eqs. (B3a)–(B3c) agree with Eqs. (2.12a)–(2.12c). This agreement illustrates the equivalence of the Feynman-diagram and difference-equation techniques for computing the numbers A_n.

APPENDIX C

Equation (2.2) gave without proof upper and lower bounds on $(-1)^{n+1}A_n$,[22] the terms in the perturbation series for the ground-state energy [Eq. (2.1)]. In this appendix, we rigorously derive these bounds using a Feynman-integral representation.

To develop the notation of the Feynman-integral representation, we restate here the ground-state-energy perturbation series [Eq. (2.1)]:

$$E_0(\lambda) = \tfrac{1}{2}m + \sum_{n=1}^{\infty} m(\lambda/m^3)^n A_n. \quad \text{(C1)}$$

A_n is the sum of all connected diagrams of order n (diagrams with n vertices) with no external legs.

---

[22] We find upper and lower bounds on $(-1)^{n+1}A_n$ because $(-1)^{n+1}A_n$ are positive quantities. This is evident from Eq. (C3).

Rewriting the perturbation series [Eq. (C1)] in terms of individual diagrams gives

$$E_0(\lambda) = \tfrac{1}{2}m + \sum_{n=1}^{\infty} m(\lambda/m^3)^n \sum I, \qquad (C2)$$

where the summation $\sum I$ is over all connected diagrams of order n with no external legs.

I is the numerical value of each diagram. In terms of a Feynman-integral representation for non-Wick-ordered connected diagrams with no external legs, I is given by

$$I = (\text{symmetry number})(\tfrac{1}{2})^w (24)^n (-1)^{n+1}$$

$$\times (1/4\pi)^{(n+1-w)/2} \Gamma(\tfrac{3}{2}n - \tfrac{1}{2}w - \tfrac{1}{2})$$

$$\times \int_0^\infty \prod_{i=1}^N \frac{dx_i}{\sqrt{x_i}} \{\delta(1 - \sum_{i=1}^N x_i)/[D(1/x_i)]^{1/2}\}. \qquad (C3)$$

In Eq. (C3), (i) $n =$ order of diagram $=$ number of vertices. In Eq. (C3), $n \geq 2$. For $n = 1$, A_1 is calculated in Appendix B. (ii) $w =$ number of lines returning to the same vertex from which they emerged (w would be zero if the interaction were Wick ordered). (iii) $N =$ number of lines $= 2n$. (iv) $x_i =$ the Feynman parameters. (v) A skeleton of a diagram is a simply connected subdiagram. $D(1/x_i) =$ the sum over all skeletons of a diagram of

$$\left(\prod_{i=1}^N \frac{1}{x_i}\right)^{-1}.$$

The product is taken over all lines in the skeleton.[23]

We use Eq. (C3) to establish bounds on $(-1)^{n+1}A_n$ by proving a sequence of theorems.

Theorem 1. Let

$$L \equiv \int_0^\infty \prod_{i=1}^N \frac{dx_i}{\sqrt{x_i}} \{\delta(1 - \sum_{i=1}^N x_i)/[D(1/x_i)]^{1/2}\}. \qquad (C4)$$

Then, (i) L is uniformly bounded above and (ii) L is uniformly bounded below. (A uniform bound on diagrams means that the bound depends only on the number of vertices and not on the individual diagrams.)

Proof of part (i). We substitute $y = \sqrt{x_i}$ into the definition of L [Eq. (C4)] and get

$$L = \int_0^\infty \prod_{i=1}^N 2dy_i \frac{\delta(1 - \sum y_i^2)}{[D(1/y_i^2)]^{1/2}}. \qquad (C5)$$

Let K_N be the surface area of a unit sphere in N dimensions. Then,

$$L \leq K_N \sup \frac{1}{[D(1/y_i^2)]^{1/2}}\bigg|_{\Sigma y_i^2 = 1}. \qquad (C6)$$

We evaluate the factors in Eq. (C6) separately.

By a straightforward evaluation of the surface-area integral, we get for the first factor

$$K_N = 2\pi^{\frac{1}{2}N}/\Gamma(\tfrac{1}{2}N). \qquad (C7)$$

In order to find the maximum of $[D(1/y_i^2)]^{-1/2}|_{\Sigma y_i^2 = 1}$, we note that $0 \leq y_i^2 \leq 1$ for each $1 \leq i \leq N$. We can overestimate a maximum by letting every $y_i = 1$. Then

$$\frac{1}{[D(1/y_i^2)]^{1/2}}\bigg|_{\Sigma y_i^2 = 1} \leq \frac{1}{\sqrt{D(1)}}$$

$$\leq \frac{1}{\sqrt{(\text{number of skeletons})}}. \qquad (C8)$$

Clearly, the smallest number of skeletons a graph could have is 1. Hence,

$$\sup \frac{1}{[D(1/y_i^2)]^{1/2}}\bigg|_{\Sigma y_i^2 = 1} = 1. \qquad (C9)$$

Combining Eqs. (C6), (C7), and (C9) and using $N = 2n$ yields

$$L \leq 2\pi^n/\Gamma(n). \qquad (C10)$$

This is the desired estimate for Theorem 1, part (i).

Proof of part (ii).[24] We make the substitution $\alpha_i = 1/x_i$ in Eq. (C4) and integrate over the δ function. The result is that

$$L = \int_0^\infty \cdots \int_0^\infty \prod_{i=2}^N \frac{d\alpha_i}{\alpha_i^{3/2}} \alpha_1^{1/2} \frac{1}{[D(\alpha_i)]^{1/2}}\bigg|_{\Sigma(1/\alpha_i) = 1}. \qquad (C11)$$

Hence,

$$L \geq \int_{2N}^{3N} \cdots \int_{2N}^{3N} \prod_{i=2}^N \frac{d\alpha_i}{\alpha_i^{3/2}} \alpha_1^{1/2} \frac{1}{[D(\alpha_i)]^{1/2}}\bigg|_{\Sigma(1/\alpha_i) = 1}. \qquad (C12)$$

So

$$L \geq \left\{\int_{2N}^{3N} \prod_{i=2}^N \frac{d\alpha_i}{\alpha_i^{3/2}}\right\} \{\inf(\sqrt{\alpha_1}) \,|\, 2N \leq \alpha_i \leq 3N\}$$

$$\times \left\{\inf \frac{1}{[D(\alpha_i)]^{1/2}}\bigg|_{\Sigma(1/\alpha_i) = 1, \, 2N \leq \alpha_i \leq 3N}\right\}. \qquad (C13)$$

We treat each of the factors in (C13) separately.

We evaluate the first factor exactly:

$$\int_{2N}^{3N} \prod_{i=2}^N \frac{d\alpha_i}{\alpha_i^{3/2}} = \left(\frac{2\sqrt{3} - 2\sqrt{2}}{(6N)^{1/2}}\right)^{N-1} \geq N^{(1-N)/2}(\tfrac{1}{10})^{N-1}. \qquad (C14)$$

The smallest possible value for the second factor is obtained when $\alpha_i = 3N$. Then,

$$\inf(\sqrt{\alpha_1}) = \left(\frac{3}{2 + 1/N}\right)^{1/2} \geq 1. \qquad (C15)$$

---

[23] Precise definitions of "skeleton" and "$D(1/x_i)$" are given in Jaffe's paper. See Ref. 4.

[24] The proof of Theorem 2, part (ii) closely follows the proof given by Jaffe. See Ref. 4. However, Jaffe's other arguments do not apply here because of counting and duplication problems associated with diagrams having no external legs.

The minimum value for the third term in Eq. (C13) is found by computing the maximum value for $D(\alpha_i)|_{\Sigma\alpha_i=1,\ 2N\leq\alpha_i\leq3N}$. But

$$\mathrm{sup}D(\alpha_i) = (\text{max number of skeletons})$$
$$\times (\text{max value for each skeleton}).\quad (C16)$$

An overestimation of the maximum number of skeletons a graph of n vertices has is 4^{n-1}. Also, the maximum value for each skeleton is achieved when all the $\alpha_i=3N$. Putting this into Eq. (C16) yields

$$\mathrm{sup}D(\alpha_i) = 4^{n-1}(3N)^{n-1}.\quad (C17)$$

Hence,

$$\inf\left\{\frac{1}{[D(\alpha_i)]^{1/2}}\Big|_{\Sigma(1/\alpha_i)=1,\ 2N\leq\alpha_i\leq3N}\right\} = (12N)^{(1-n)/2}.$$
$$(C18)$$

We combine Eqs. (C14), (C15), and (C18) with Eq. (C13) to get

$$L\geq (N^{(1-N)/2})(\tfrac{1}{10})^{N-1}(12N)^{(1-n)/2}.\quad (C19)$$

Substituting $N=2n$,

$$L\geq (2n)^{(1-2n)/2}(10)^{1-2n}(24n)^{(1-n)/2}.\quad (C20)$$

This is the desired estimate for Theorem 1, part (ii). Note that the bounds given in Eq. (C10) and in Eq. (C20) are uniform. That is, they depend on n but not on the individual diagrams.

Theorem 2. The symmetry number for diagrams is uniformly bounded (i) above and (ii) below.

Proof of part (i). Since all symmetry numbers are less than 1, an upper bound on symmetry numbers for all diagrams is 1.

Proof of part (ii). A small symmetry number corresponds to a diagram having much symmetry. The class of connected diagrams having the greatest degree of symmetry per number of vertices is shown in Fig. 7. If n is the number of vertices, the symmetry numbers for diagrams belonging to this infinite class is exactly

$$\mathrm{S.N.} = 1/(8\times6^{n/2}).\quad (C21)$$

Equation (C21) serves as a lower bound on all symmetry numbers. This completes Theorem 2.

Combining the results of Theorems 1 and 2 places upper and lower bounds on $(-1)^{n+1}I$. Those bounds are

$$(-1)^{n+1}I\leq(\tfrac{1}{2})^w(24)^n\left(\frac{1}{(4\pi)^{1/2}}\right)^{n+1-w}$$
$$\times\Gamma(\tfrac{3}{2}n-\tfrac{1}{2}w-\tfrac{1}{2})\frac{2\pi^n}{\Gamma(n)}\quad (C22)$$

and

$$(-1)^{n+1}I\geq\frac{1}{8}\frac{1}{6^{n/2}}(\tfrac{1}{2})^w(24)^n\left(\frac{1}{(4\pi)^{1/2}}\right)^{n+1-w}$$
$$\times\Gamma(\tfrac{3}{2}n-\tfrac{1}{2}w-\tfrac{1}{2})(2n)^{(1-2n)/2}\times10^{1-2n}(24n)^{(1-n)/2}.\quad (C23)$$
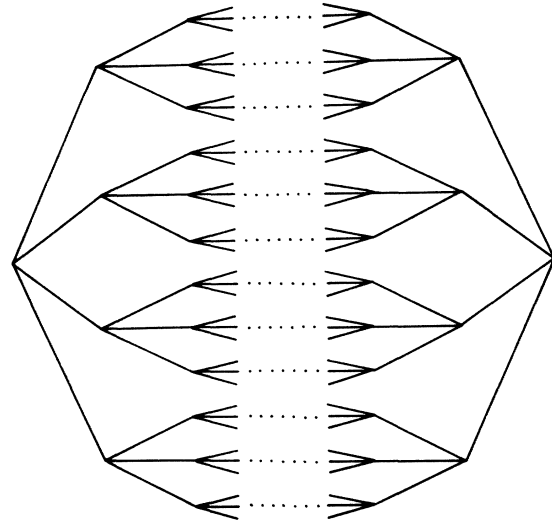

FIG. 7. The infinite class of diagrams having maximum symmetry per number of vertices. These diagrams have the smallest symmetry numbers for diagrams with a comparable number of vertices. All diagrams in this class start from a single vertex, each of whose four lines branches repeatedly and symmetrically into three new lines; after an arbitrary number of branchings, the lines symmetrically recombine into a single vertex.

To find bounds on $(-1)^{n+1}A_n$, we must make the estimates for $(-1)^{n+1}I$ independent of w. Clearly, for a connected diagram of n vertices, w can range from 0 to n. Therefore, in Eq. (C22) we take $w=0$ and in Eq. (C23) we take $w=n$. After simplification, the estimates [Eqs. (C22) and (C23)] become

$$(-1)^{n+1}I\leq\frac{1}{\sqrt{\pi}}(12\sqrt{\pi})^n\frac{\Gamma(\tfrac{3}{2}n-\tfrac{1}{2})}{\Gamma(n)}\quad (C24)$$

and

$$(-1)^{n+1}I\geq\frac{5}{2}\left(\frac{3}{\pi}\right)^{1/2}\left(\frac{1}{200}\right)^n\Gamma(n-\tfrac{1}{2})n^{(2-3n)/2}.\quad (C25)$$

We now return to the integral representation [Eq. (C3)] and observe that for a given order n the contributions from all diagrams add in phase. Therefore, upper and lower bounds on $(-1)^{n+1}A_n$, the terms in the perturbation series, may be obtained once we place bounds on the number of diagrams in each order.

Theorem 3. The number of diagrams of order n is (i) bounded above by $(4n-1)!!$ and (ii) bounded below by $n!/3^n$.

Proof of part (i). We establish an upper bound on the number of diagrams by constructing them as follows.

We begin with n vertices. None of the vertices are connected, so each has four free lines emerging from it. There are $4n$ free lines.

We pick any line and connect it to one of the other $4n-1$ lines. There are now $4n-2$ lines. We pick and connect another line in one of $4n-3$ ways. We continue until there are no free lines. Therefore, there are at most $(4n-1)!!$ diagrams.

Proof of part (ii). In order to establish a lower bound on the number of diagrams, we establish a lower bound on the number of diagrams belonging to a particular class. We consider only those diagrams in which all the vertices lie on a continuous closed line (a circular path). We construct such a class of diagrams as follows.

Draw a circle and place all the n vertices on it. The circle uses up two of the four lines at each vertex. This leaves two free (unconnected) lines extending from every vertex. Now start with any vertex and pick one of the two free lines emerging from it. Join this line to a line coming from any of the n vertices (including itself). Connect the last free line coming from this new vertex to one of the remaining $n-1$ vertices. Continue this process, going sequentially from vertex to vertex until all pairs of free lines are used up. Since we use both lines at each vertex one right after the other, the number of available vertices keeps decreasing by one. Of course, at any time the process may close on itself if the free line is connected to the last line available at the original vertex. If this happens, we simply start over at any other free vertex, which will have two available lines, and continue.

Clearly, there are $n!$ ways to carry out the above process, but there will be many duplications. To avoid these duplications, we divide by three at each vertex.

We conclude that there are at least $n!/3^n$ diagrams. This establishes Theorem 3.

Combining the results of Theorem 3 with Eqs. (C24) and (C25) places upper and lower bounds on $(-1)^{n+1}A_n$:

$$(-1)^{n+1}A_n \leq \frac{(4n-1)!!\Gamma(\frac{3}{2}n-\frac{1}{2})}{\Gamma(n)} \frac{(12\sqrt{\pi})^n}{\sqrt{\pi}} \quad \text{(C26)}$$

and

$$(-1)^{n+1}A_n \geq \frac{n!\Gamma(n-\frac{1}{2})}{n^{(3n-2)/2}}(600)^{-n}\left(\frac{5}{2}\sqrt{\frac{3}{\pi}}\right)^{1/2}. \quad \text{(C27)}$$

Simplifying Eqs. (C26) and (C27) yields

$$AB^n\Gamma(\tfrac{1}{2}n) \leq (-1)^{n+1}A_n \leq CD^n\Gamma(\tfrac{5}{2}n). \quad \text{(C28)}$$

Equation (C28) is the final result. Note that it agrees with the bounds in Eq. (2.2).

APPENDIX D

In this appendix, we discuss the details of the computer calculation of the first 75 terms in the ground-state-energy perturbation series [Eq. (2.1)] which is

$$E_0(\lambda) = \tfrac{1}{2}m + \sum_{n=1}^{\infty} mA_n(\lambda/m^3)^n. \quad \text{(D1)}$$

In the calculation, the difference equation [Eq. (2.8)]

which is

$$2jB_{i,j} = (j+1)(2j+1)B_{i,j+1} + B_{i-1,j-2}$$

$$-\sum_{p=1}^{i-1} (B_{i-p,1})(B_{p,j}) \quad \text{(D2)}$$

and Eq. (2.9) which is

$$A_i = -B_{i,1} \quad \text{(D3)}$$

were used on an IBM 7094 in double-precision mode. (The results of this computer calculation are listed in Table I. The absolute value of A_n is listed to the right of the order n. The number following the comma is the power of 10 multiplying the decimal.)

The computer program had three interesting features.

(i) To calculate A_n it was necessary to know all $B_{i,j}$ for $j = 1, 2, \cdots, 2n$ and $i = 1, \cdots, n$. Because $B_{i,j}$ has two indices, the limiting factor in this calculation was not time but memory capacity. Seventy-five was the maximum number of terms in the perturbation series

TABLE I. The absolute values of the first 75 terms A_n in the perturbation series for the ground-state energy [Eq. (2.1)]. The number following the comma is the power of 10 multiplying the decimal. The signs of A_n alternate beginning with plus, i.e., $A_n = (-)^{n-1}|A_n|$.

n	$|A_n|$		n	$|A_n|$	
1	0.750000000000,	0	39	0.559961162001,	64
2	0.262500000000,	1	40	0.664186377517,	66
3	0.208125000000,	2	41	0.807715625319,	68
4	0.241289062500,	3	42	0.100646863922,	71
5	0.358098046875,	4	43	0.128429408835,	73
6	0.639828134766,	5	44	0.167730490075,	75
7	0.132973372705,	7	45	0.224085871222,	77
8	0.314482146928,	8	46	0.306093131234,	79
9	0.833541603263,	9	47	0.427287814796,	81
10	0.244789407028,	11	48	0.609277658120,	83
11	0.789333316003,	12	49	0.887045954492,	85
12	0.277387769635,	14	50	0.131804184041,	88
13	0.105564665831,	16	51	0.199796510697,	90
14	0.432681068354,	17	52	0.308853507485,	92
15	0.190081719760,	19	53	0.486698406263,	94
16	0.891210175364,	20	54	0.781543229859,	96
17	0.444255088999,	22	55	0.127844051221,	99
18	0.234646430681,	24	56	0.212959346691,	101
19	0.130915026105,	26	57	0.361127834038,	103
20	0.769399985382,	27	58	0.623214611884,	105
21	0.475124077343,	29	59	0.109419743747,	108
22	0.307579295113,	31	60	0.195392812615,	110
23	0.208301009434,	33	61	0.354775753462,	112
24	0.147290492138,	35	62	0.654807077714,	114
25	0.108552296005,	37	63	0.122820914441,	117
26	0.832483627531,	38	64	0.234056056576,	119
27	0.663329371112,	40	65	0.453052532884,	121
28	0.548392431330,	42	66	0.890541554378,	123
29	0.469782420784,	44	67	0.177719768349,	126
30	0.416502699806,	46	68	0.359993943833,	128
31	0.381734895502,	48	69	0.740009711275,	130
32	0.361299554016,	50	70	0.154336989562,	133
33	0.352778001982,	52	71	0.326515091790,	135
34	0.355023393768,	54	72	0.700567351807,	137
35	0.367917476478,	56	73	0.152414090414,	140
36	0.392301600257,	58	74	0.336160314738,	142
37	0.430055097492,	60	75	0.751507982642,	144
38	0.484327278330,	62			

which could be computed without using additional memory space on disks or tapes.

(ii) The numbers $B_{i,j}$ grow exponentially large or small with i for j near 1 or near $2i$. As a result, the capacity of the 7094 to manipulate these large and small exponents in floating point would be exceeded before $i=20$. Therefore, it was necessary to scale the $B_{i,j}$. One particularly useful scaling is

$$C_{i,j}=(1/100^{i-j})B_{i,j}. \tag{D4}$$

Equation (D4) is adequate for $n \lesssim 100$.

(iii) The structure of the difference equation [Eq. (D2)] indicated that a huge number of manipulations would have to be performed in which numbers with greatly differing exponents would be added together. This would cause round-off errors which on a computer are cumulative. Therefore, although the calculation was done to 16 decimal places (double-precision mode), one must take care to determine the number of decimal places which are really significant.

If we assume that the round-off errors are purely random (not systematic), then the cumulative error grows as the square root of the number of operations. Because there are approximately 10^8 operations performed in the calculation of A_{75}, we expect that the error is about 10^4 in 10^{16}. That is, the last four decimal places (of the sixteen) are random.

We can check that there are indeed 12 significant figures in the table of A_n as follows: Divide out the dominant asymptotic behavior of the A_n [see Eq. (2.10)] and make a table of the resulting numbers Q_n:

$$Q_n \equiv \frac{A_n}{(\sqrt{6})\pi^{-3/2}\Gamma(n+\frac{1}{2})3^n}. \tag{D5}$$

Then compute a table of the successive differences:

$$Q_n^{(1)} \equiv Q_n - Q_{n-1}, \tag{D6a}$$

$$Q_n^{(2)} \equiv Q_n^{(1)} - Q_{n-1}^{(1)}, \tag{D6b}$$

and so on.

The $Q_n^{(i)}$ are regularly monotonic as i increases until they become random. By inspection we find that $Q^{(9)}$ is random and, as expected, it is nonzero in the last four decimal places (of the sixteen). This verifies that the Q_n and hence the A_n are correct to 12 places.

APPENDIX E

There is no known mathematically rigorous proof of the detailed asymptotic growth of the A_n as given in Eq. (2.10). However, in this appendix, we justify this equation using numerical methods. The raw data used in this appendix are contained in Table I.

We approach the problem by finding the rough growth of A_n. To do this, we construct a table of the ratios

$$R_n = A_{n+1}/A_n \tag{E1}$$

from the values of A_n listed in Table I. As $n \to 75$, we observe that to a good approximation $R_n \to 3(n+\frac{1}{2})$. This indicates that A_n grows as $3^n\Gamma(n+\frac{1}{2})$.

Next we try to fit A_n very accurately by

$$A_n \sim 3^n\Gamma(n+\tfrac{1}{2})\left(a_0+\frac{a_1}{n}+\frac{a_2}{n^2}+\frac{a_3}{n^3}+\cdots\right). \tag{E2}$$

[The $\sim$ notation in Eq. (E2) is justified because the term in square brackets is an asymptotic (nonconvergent) series.] Note that it would not be possible to fit A_n by a series such as that in Eq. (E2) if A_n did not grow as $3^n\Gamma(n+\frac{1}{2})$; that is, if the rough growth of A_n were, say, $(2.9)^n\Gamma(n+\frac{1}{2})$ or $3^n\Gamma(n+0.6)$.

To evaluate the a_i in Eq. (E2), we use Table I to calculate

$$P_n = A_n/3^n\Gamma(n+\tfrac{1}{2}). \tag{E3}$$

Then we terminate the series in Eq. (E2) at a_k and solve for a_i, $i=0, 1, \cdots, k$, in the resulting set of simultaneous equations:

$$P_n = a_0 + \frac{a_1}{n} + \frac{a_2}{n^2} + \cdots + \frac{a_k}{n^k}, \tag{E4}$$

where $n = 75-k, \; 75-k+1, \; \cdots, \; 75$.

We solve for a_0 in Eq. (E4) by multiplying each equation by n^k, taking successive differences, and using the beautiful identity:

$$\sum_{i=0}^{k} (n-i)^k \binom{k}{i}(-1)^i = k!. \tag{E5}$$

a_0 may thus be given exactly in closed form by

$$a_0 = \sum_{i=0}^{k} (-1)^i P_{75-i} \binom{k}{i}(75-i)^k \Big/ k!. \tag{E6}$$

Once a_0 is known, we can reduce Eq. (E4) to a new set of equations in which P_n is replaced by $(P_n-a_0)n$ and k by $k-1$. We solve as before for the new a_0 which is the old a_1. Repeating this process k times gives all a_i.

If we terminate the series at a_5, we find that to four parts in 10^9

$$a_0 = (\sqrt{6})/\pi^{3/2}. \tag{E7}$$

We also find that

$$a_1/a_0 = 1.3194528, \tag{E8a}$$

$$a_2/a_0 = 1.9366649, \tag{E8b}$$

$$a_3/a_0 = 7.1004516, \tag{E8c}$$

$$a_4/a_0 = 27.445970, \tag{E8d}$$

$$a_5/a_0 = 665.57303. \tag{E8e}$$

Apparently, as i increases, the growth of the numbers a_i is so rapid that when $n \sim 75$, the term a_6/n^6 is larger than a_5/n^5. This suggests that the asymptotic series

in Eq. (E4) is an optimal approximation of P_n when it is terminated at a_5/n^5. (More terms could be included, giving a more accurate approximation to P_n, only if n were larger.)

Since we keep six terms in the asymptotic series, we expect that P_n should be represented accurately and uniformly to a few parts in 10^9. This turns out to be the case for n near 75 down to well below 50. Because a_0 is $(\sqrt{6})\pi^{-3/2}$ to four parts in a billion and since the magnitude of this error is exactly what we would expect, we assert that a_0 *is* $(\sqrt{6})\pi^{-3/2}$.

Combining this value for a_0 with Eq. (E2) gives Eq. (2.10) which is the result we had set out to derive in this appendix, namely,

$$A_n \sim 3^n \Gamma(n+\tfrac{1}{2})(\sqrt{6})\pi^{-3/2}. \tag{E9}$$

One might note that although a_0 is known to four parts in 10^9, a_i/a_0 in Eq. (E8) is known less and less accurately as i increases. a_1/a_0 is accurate to seven or eight places; a_2/a_0 is accurate to five or six places; and a_5/a_0 is accurate to one place at most.

To increase the accuracy of a_i, A_n would have to be calculated for n much larger than 75. As is always the case with asymptotic series, nothing is gained by calculating A_n more precisely for n near 75.

Aside from simplicity, there is no compelling reason why P_n should be expanded into an asymptotic series of the form in Eq. (E2). One might prefer to use the more general series

$$P_n \sim \alpha_0 + \frac{\alpha_1}{(n+\epsilon)} + \frac{\alpha_2}{(n+\epsilon)^2} + \frac{\alpha_3}{(n+\epsilon)^3} + \cdots, \tag{E10}$$

where ϵ is any number which is small compared to n. Then a simple formula relates the a_i to the α_i:

$$\alpha_0 = a_0, \tag{E11a}$$

$$\alpha_1 = a_1, \tag{E11b}$$

$$\alpha_2 = a_2 + \epsilon a_1, \tag{E11c}$$

$$\alpha_3 = a_3 + 2\epsilon a_2 + \epsilon^2 a_1, \tag{E11d}$$

$$\alpha_4 = a_4 + 3\epsilon a_3 + 3\epsilon^2 a_2 + \epsilon^3 a_1, \tag{E11e}$$

and, in general,

$$\alpha_n = \sum_{i=1}^{n} a_i \epsilon^{n-i} \binom{n-1}{i-1}. \tag{E11f}$$

This completes our remarks on these numerical calculations. However, before concluding this appendix, we will discuss an example of how investigations of this sort might lead to a better understanding of the singularity structure of the ground-state energy $E_0(\lambda)$ in the complex plane.

Example. As a crude illustration of how one might recover the analytic properties of $E_0(\lambda)$ from Eq. (E2),

we neglect a_i for $i \geq 1$. Then Eqs. (E2) and (2.1) give

$$E_0(\lambda) \sim \sum_{n=0}^{\infty} \lambda^n (-1)^n (\sqrt{6})\pi^{-3/2}\Gamma(n+\tfrac{1}{2})3^n. \tag{E12}$$

Then, ignoring the possibility that two unequal functions can have the same asymptotic expansion, we substitute the expression

$$\Gamma(n+\tfrac{1}{2}) = \int_0^\infty e^{-t} t^{n-\frac{1}{2}} dt \tag{E13}$$

into Eq. (E12). Interchanging summation and integration, summing the series, and letting $s = \sqrt{t}$ gives a convergent integral representation for E_0:

$$E_0(\lambda) \cong \frac{2\sqrt{6}}{\pi^{3/2}} \int_0^\infty \frac{e^{-s^2}}{1+3\lambda s^2} ds. \tag{E14}$$

For λ real and positive, this integral can be evaluated explicitly with the result that

$$E_0(\lambda) \cong (2/\pi\lambda)^{1/2} \exp(1/3\lambda) \, \mathrm{Erfc}[(3\lambda)^{-1/2}], \tag{E15}$$

where

$$\mathrm{Erfc}(x) = \frac{2}{\sqrt{\pi}} \int_0^\infty e^{-t^2} dt. \tag{E16}$$

More importantly, the dispersion-type integral in Eq. (E14) defines a nontrivial singularity structure in the λ plane—a cut along the negative real λ axis. The jump across the cut is easily calculated. Unfortunately, this result does not come close to giving the true singularity structure of $E_0(\lambda)$ as derived in Secs. III, IV, and VI of this paper. Nevertheless, it is hoped that future calculations of this sort will lead to positive results.

APPENDIX F

In this appendix, we present the WKB calculation of Eq. (4.35) to first order in λ. A successful calculation would be a significant result because:

(i) Our continued ability to match the asymptotic expansions across the boundaries in regions A, B, C, and D would give added assurance that the application of WKB techniques to the problem of locating singularities in $E(\lambda)$ is valid.

(ii) It is most important to make sure that the first-order result we obtain here differs from the zeroth-order result only by terms of order λ. This would imply that the error in Eq. (4.35) is indeed small, as is tacitly assumed in Secs. IV, V, and VI.

(iii) As a byproduct, this calculation would define the boundaries of regions A, B, C, and D more precisely than the zeroth-order calculation does. This added precision would result from the greater number of terms that would be matched across the boundaries.

In this appendix, we will follow the same procedure as in the zeroth-order calculation in Sec. IV. However, we keep terms of order λ as well as of order 1. We neglect terms of order λ^2 or smaller. We again use the differential equation [Eq. (4.9)] which is

$$[d^2/dr^2 + \tfrac{1}{4}(-\epsilon + r^2 - \rho r^4)]\Phi(r) = 0,\qquad (F1)$$

and recall the definitions $\rho = \lambda e^{-3\pi i/2}$, $\epsilon = 4iE$, and $r = xe^{i\pi/4}$.

We define the four regions A, B, C, and D as in Sec. IV. That is, in region A, $0 < |r| \ll |r_0|$; in region B, $|r_0| \ll |r| \ll |r_1|$; in region C, $|r_0| \ll |r| \lesssim |r_1|$; and in region D, $|r| \sim |r_1|$.

Also, for the first-order calculation r_0 and r_1 must be given more exactly than for the zeroth-order calculation. From Eq. (4.10), we have

$$r_0 = \{[1 - (1-4\rho\epsilon)^{1/2}](2\rho)^{-1}\}^{1/2} \sim (\sqrt{\epsilon})(1 + \tfrac{1}{2}\rho\epsilon) \quad (F2a)$$

and

$$r_1 = \{[1 + (1-4\rho\epsilon)^{1/2}](2\rho)^{-1}\}^{1/2}$$
$$\sim (1/\sqrt{\rho})(1 - \tfrac{1}{2}\rho\epsilon). \quad (F2b)$$

As in Sec. IV, we consider separately the regions A, B, C, and D.

Region A. We solve Eq. (F1) to first order in λ. To do this for region A, we find a transformation which to first order in λ turns Eq. (F1) into a parabolic cylinder function differential equation.[25] The transformation which works is

$$w = x + \lambda(\tfrac{1}{8}x^3 + \tfrac{3}{4}Ex). \quad (F3)$$

Then, the even-parity solution to (D1) is

$$\Phi_A = C(1 - \tfrac{3}{16}\lambda x^2)[D_\nu(w) + D_\nu(-w)], \quad (F4)$$

where

$$\nu = E - \tfrac{1}{2} - \tfrac{3}{2}\lambda(E^2 + \tfrac{1}{4}). \quad (F5)$$

[In this appendix, we do the WKB calculation for even-parity wave functions only. The differences for odd parity involve the algebraic manipulations in region A.]

We compute the asymptotic expansion of Φ_A in region A for r near region B. The first two terms in the asymptotic expansion[26] for $D_\nu(w)$ are

$$D_\nu(w) \sim w^\nu e^{-\tfrac{1}{4}w^2}\left[1 + \frac{\nu(1-\nu)}{2w^2}\right]$$

$$\text{for } -\tfrac{3}{4}\pi < \arg w < \tfrac{3}{4}\pi \quad (F6a)$$

and

$$D_\nu(w) \sim w^\nu e^{-\tfrac{1}{4}w^2}\left[1 + \frac{\nu(1-\nu)}{2w^2}\right] - \frac{(2\pi)^{1/2}}{\Gamma(-\nu)}$$

$$\times e^{\nu\pi i}w^{-\nu-1}e^{\tfrac{1}{4}w^2}\left[1 + \frac{(1+\nu)(2+\nu)}{2w^2}\right]$$

$$\text{for } \tfrac{1}{4}\pi < \arg w < (5/4)\pi. \quad (F6b)$$

Equations (F2)–(F6) are used to expand Φ_A into its asymptotic form. We expand to first order in powers of ρ and r_0^2/r^2. We keep terms of the form ρ and r_0^2/r^2 and neglect terms of the form ρ^2, $\rho r_0^2/r^2$, and r_0^4/r^4. These approximations are justified because they give the correct asymptotic connection with Φ_B. As we had expected, these approximations define the extent of region A more clearly than the zeroth-order calculation did.

After considerable simplification,[27] the asymptotic expansion for Φ_A is

$$\Phi_A \sim C 2\pi 2^{\tfrac{1}{2}\nu+\tfrac{1}{4}}e^{\pi i/8}e^{\pi i\nu/4}\left(1 + \frac{3\rho r^2}{16}\right)\left(1 + \frac{\epsilon}{4r^2} + \frac{\rho r^2}{16} + \frac{17\rho\epsilon}{64}\right)\left[1 - \frac{\rho\epsilon}{32}\left(\frac{37}{8} + \frac{\epsilon^2}{32}\right)\right]$$

$$\times \left\{\frac{r^\nu}{\Gamma(\tfrac{1}{2}+\tfrac{1}{2}\nu)}\exp\left[\frac{ir^2}{4}\left(1 - \frac{3\rho\epsilon}{8} - \frac{\rho r^2}{4}\right) - \frac{i\pi}{8}\right]\exp\left[\frac{i}{4}\left(\frac{3\rho\epsilon^2}{16} + \frac{\rho\epsilon r^2}{8} + \frac{\epsilon^2}{8r^2} - \frac{2}{2r^2}\right)\right]2^{-\tfrac{1}{2}\nu-\tfrac{1}{4}}\right.$$

$$\left. + \frac{r^{-\nu-1}}{\Gamma(-\tfrac{1}{2}\nu)}\exp\left[\frac{-ir^2}{4}\left(1 - \frac{3\rho\epsilon}{8} - \frac{\rho r^2}{4}\right) + \frac{i\pi}{8}\right]\exp\left[-\frac{i}{4}\left(\frac{3\rho\epsilon^2}{16} + \frac{\rho\epsilon r^2}{8} + \frac{\epsilon^2}{8r^2} - \frac{3}{2r^2}\right)\right]2^{\tfrac{1}{2}\nu+\tfrac{1}{4}}\right\}. \quad (F7)$$

This is the desired result for region A.

Region B. The first-order WKB solution[28] to the differential equation [Eq. (F1)] is

$$\Phi_{\text{WKB}} = \frac{\sqrt{\mu}}{(1 - \tfrac{1}{8}\mu'^2 + \tfrac{1}{4}\mu''\mu)^{1/2}}\left(C_2\exp\left\{i\left[\int^r\left(\frac{1}{\mu} - \frac{\mu'^2}{8\mu}\right)dr + \frac{\mu'}{4}\right]\right\}C_3\exp\left\{-i\left[\int^r\left(\frac{1}{\mu} - \frac{\mu'^2}{8\mu}\right)dr + \frac{\mu'}{4}\right]\right\}\right), \quad (F8)$$

---

[25] BMP, Vol. 2, p. 116, Eq. (1).

[26] BMP, Vol. 2, pp. 116–123. There is a serious misprint not on the errata sheet which must be corrected before one can do the first-order WKB calculation. Equation (2), p. 123, should read

$$D_\nu(z) = z^\nu e^{-z^2/4}\left[\sum_{n=0}^N \frac{(-\tfrac{1}{2}\nu)_n(\tfrac{1}{2}-\tfrac{1}{2}\nu)_n}{n!(-z^2/2)^n} + O|z^2|^{-N-1}\right] - \frac{(2\pi)^{1/2}}{\Gamma(-z)}e^{\nu\pi i}z^{-\nu-1}e^{z^2/4}\left[\sum_{n=0}^N \frac{(1+\tfrac{1}{2}\nu)_n(\tfrac{1}{2}+\tfrac{1}{2}\nu)_n}{n!(z^2/2)^n} + O|z^2|^{-N-1}\right] \text{ for } \pi/4 < \arg z < 5\pi/4.$$

Equation (3), p. 123, has a similar misprint but it is not needed in this paper. The equation is derived correctly in E. T. Whittaker and G. N. Watson, *A Course of Modern Analysis* (Cambridge University Press, Cambridge, 1952).

[27] BMP, Vol. 1, pp. 1–5.

[28] See Ref. 8. For first-order WKB techniques, see A. Messiah, pp. 233–234.

where

$$\mu = 2(-\epsilon + r^2 - \rho r^4)^{-1/2}. \tag{F9}$$

We would encounter a serious difficulty with this first-order calculation if we were to proceed as we did in Sec. IV. If we fixed the constants C_2 and C_3 in Eq. (F8) by defining the lower endpoint (the reference point) in the integrals to be r_0, we would find that the integrals become divergent regardless of the upper endpoint. The same would be true if we picked r_1 to be the reference point. In order to avoid this difficulty, we carry out the following procedure.

We treat $-\frac{1}{8} \int dr \, \mu'^2/\mu$ as an indefinite integral and integrate by parts repeatedly. This isolates the divergences at $r = r_0$ and r_1. After some tedious algebra, the result is

$$-\frac{1}{8} \int^r dr \frac{\mu'^2}{\mu} = -\frac{1}{6}\left(\rho r^3 - \frac{r}{2}\right)(-\epsilon + r^2 - \rho r^4)^{-3/2}$$

$$-\frac{1}{12\epsilon(1-4\rho\epsilon)}(-\epsilon + r^2 - \rho r^4)^{-1/2}$$

$$\times [\rho r^3(1-12\rho\epsilon) - r(1-8\rho\epsilon)]$$

$$+\frac{\rho}{12\epsilon(1-4\rho\epsilon)}\int_{r_0}^r \frac{4\epsilon + (1-12\rho\epsilon)r^2}{(-\epsilon + r^2 - \rho r^4)^{1/2}}dr + \text{const}. \tag{F10}$$

In Eq. (F10),

$$\epsilon = r_1^2 r_0^2/(r_1^2 + r_0^2), \tag{F11}$$

$$\rho = (r_1^2 + r_0^2)^{-1}. \tag{F12}$$

Equation (F10) is an exact equation. Equations (F11) and (F12) are also exact and follow from the definitions of r_0 and r_1 [Eq. (4.10)].

We determine the constant in Eq. (F10) to first order by evaluating the integral $-\frac{1}{8}\int^r dr \, \mu'^2/\mu$ using a second method. Using Eq. (F9), we have

$$\int^r -\frac{1}{8}\frac{\mu'^2}{\mu}dr$$

$$= -\int^r dr(-\epsilon + r^2 - \rho r^4)^{-5/2}(\rho r^3 - \frac{1}{2}r)^2. \tag{F13}$$

Expanding the right-hand side of Eq. (F13) in region B to first order, we find that

$$\int^r -\frac{1}{8}\frac{\mu'^2}{\mu}dr \sim -\frac{1}{4}\int^r dr\left(r^{-3} + \frac{5}{2}\epsilon r^{-5} - \frac{3}{2}\rho r^{-1} - \frac{5}{4}r^{-3}\rho\epsilon\right)$$

$$\sim \frac{1}{8r^2} + \frac{3\rho}{8}\ln\frac{2r}{r_0}. \tag{F14}$$

As in region A, the first-order asymptotic expansion in region B means that we expand in powers of ρ and and r_0^2/r^2. We keep terms of the form ρ and r_0^2/r^2 and neglect terms of the form r_0^4/r^4, ρ/r^2, and ρ^2.

Finally, we return to Eq. (F10) and approximate that equation to first order in region B with the result that

$$\int^r -\frac{1}{8}\frac{\mu'^2}{\mu}dr \sim \text{const} + \frac{1}{8r^2} + \frac{3\rho}{8}\ln\frac{2r}{r_0} + \frac{1}{12\epsilon} - \frac{3\rho}{8}. \tag{F15}$$

Comparing Eqs. (F14) and (F15) determines that the constant in Eq. (F13) gives

$$\text{const} = 3\rho/8 - 1/12\epsilon. \tag{F16}$$

We have thus avoided the divergences which come from the endpoints in the evaluation of $-\frac{1}{8}\int dr \, \mu'^2/\mu$. As a result, Eq. (F10) with the constant of integration given in Eq. (F16) is a well-defined and consistent integral evaluation valid in both regions B and C. Hence, the constants C_2 and C_3 are fixed.

We now calculate to first order the asymptotic expansion of Φ_{WKB} [Eq. (F8)] in region B.

First, we expand $\frac{1}{4}\mu'$.

$$\tfrac{1}{4}\mu' = (-\epsilon + r^2 - \rho r^4)^{-3/2}(\rho r^3 - \tfrac{1}{2}r) \tag{F17}$$

$$\sim -\frac{1}{2r^2} + \frac{\rho}{4}. \tag{F18}$$

Second, we expand $(1 - \frac{1}{8}\mu'^2 + \frac{1}{4}\mu\mu'')^{-1/2}$ to first order and get simply

$$(1 - \tfrac{1}{8}\mu'^2 + \tfrac{1}{4}\mu\mu'')^{-1/2} \sim 1. \tag{F19}$$

Third, we expand $\sqrt{\mu}$. To first order,

$$\sqrt{\mu} \sim \left(\frac{2}{r}\right)^{1/2}\left(1 + \frac{3}{16}\rho r^2\right)\left(1 + \frac{\epsilon}{4r^2} + \frac{\rho r^2}{16} + \frac{17\rho\epsilon}{64}\right). \tag{F20}$$

Fourth, we must evaluate $\int_{r_0}^r (1/\mu)dr$. Note that there is no difficulty with endpoint divergences in this integral. Therefore, we treat it just as we did in Sec. IV except that we retain first-order terms. From Eq. (F9), we have

$$\int_{r_0}^r \frac{1}{\mu}dr = \frac{1}{2}\int_{r_0}^r (-\epsilon + r^2 - \rho r^4)^{1/2}dr. \tag{F21}$$

We expand the integral in Eq. (F21) and get

$$\int_{r_0}^r \frac{1}{\mu}dr \sim \frac{\sqrt{\rho}}{2}\int_{r_0}^r dr(r^2 - r_0^2)^{1/2}r_1 - \left(\frac{r^2}{2r_1}\right). \tag{F22}$$

Substituting $r = r_0 \cosh\Theta$ into Eq. (F22) and integrating gives

$$\int_{r_0}^r \frac{1}{\mu}dr \sim \frac{1}{4}\left\{-\epsilon\left(1 + \frac{3}{8}\rho\epsilon\right)\ln\frac{2r}{r_0} + r^2\left(1 - \frac{1}{4}\rho\epsilon\right)\right.$$

$$\left. -\frac{r^4\rho}{4} - \frac{1}{2}\epsilon\left(1 + \frac{9}{16}\rho\epsilon\right) + \frac{\epsilon^2}{8r^2}\right\}. \tag{F23}$$

We combine Eqs. (F14), (F18)–(F20), and (F23). These five results are needed to give us the asymptotic expansion of Φ_{WKB} (F8) in region B:

$$\Phi_B \sim \left(\frac{2}{r}\right)^{1/2}\left(1+\frac{3}{16}\rho r^2\right)\left(1+\frac{\epsilon}{4r^2}+\frac{\rho r^2}{16}+\frac{17\rho\epsilon}{64}\right)$$

$$\times\left(C_2 \exp\left\{i\left[\frac{1}{4}\left(-\epsilon(1+\tfrac{3}{8}\rho\epsilon)\ln\frac{2r}{r_0}+r^2(1-\tfrac{1}{4}\rho\epsilon)-\tfrac{1}{4}r^4\rho\right.\right.\right.\right.$$

$$\left.\left.\left.-\tfrac{1}{2}\epsilon\left(1+\frac{9}{16}\rho\epsilon\right)+\frac{\epsilon^2}{8r^2}\right)-\frac{1}{2r^2}+\frac{\rho}{4}+\frac{1}{8r^2}+\frac{3\rho}{8}\ln\frac{2r}{r_0}\right]\right\}$$

$$+C_3 \exp\{-i[\cdots]\}\Big).\quad (F24)$$

Region C. We calculate to first order the asymptotic expansion of Φ_{WKB} [Eq. (F8)] in region C. For this purpose it is convenient to use a new variable R:

$$R \equiv r_1 - r_0.\quad (F25)$$

Expansions in region C are done in powers of ρ and R/r_1. For first order we keep terms of the form ρ and R/r_1 and neglect terms of the form R^2/r_1^2, $R\rho/r_1$, and ρ^2.

The components of the asymptotic expansion of Φ_{WKB} [Eq. (F8)] are computed in turn:
First,

$$\mu^{1/2} \sim \frac{2^{1/4}\rho^{1/8}}{R^{1/4}}\left[1+\frac{\rho}{4}\left(\frac{5}{2}\epsilon+\frac{5}{2}\frac{R}{\rho^{1/2}}\right)\right].\quad (F26)$$

Second, as in region B,

$$(1-\tfrac{1}{8}\mu'^2+\tfrac{1}{4}\mu''\mu)^{-1/2}\sim 1.\quad (F27)$$

Third,

$$\tfrac{1}{4}\mu' \sim \frac{R^{-3/2}\rho^{1/4}}{24\sqrt{2}}\left(6+\frac{15}{2}\rho\epsilon-\frac{15}{2}R\sqrt{\rho}\right).\quad (F28)$$

Fourth, we decompose the integral $\int_{r_0}^{r}(1/\mu)dr$ as follows:

$$\int_{r_0}^{r}\frac{1}{\mu}dr=\int_{r_0}^{r_1}\frac{1}{\mu}dr-\int_{r}^{r_1}\frac{1}{\mu}dr.\quad (F29)$$

The first integral in Eq. (F29) will be expressed later in terms of elliptic integrals [see Eq. (F47)]. For now we label it P:

$$P=\int_{r_0}^{r_1}\frac{1}{\mu}dr.\quad (F30)$$

The second integral in Eq. (F29) may be approximated easily, with the result that

$$-\int_{r}^{r_1}\frac{1}{\mu}dr\sim -\tfrac{1}{2}\sqrt{3}\rho^{-1/4}R^{3/2}\left(1-\frac{5}{4}\rho\epsilon-\frac{3}{4}(\sqrt{\rho})R\right).\quad (F31)$$

Fifth, we use Eq. (F10) to approximate $\int-\tfrac{1}{8}(\mu'^2/\mu)dr$. We decompose the integral in Eq. (F10) using the same

method as in Eq. (F29) and define the definite integral as Q:

$$Q=\int_{r_0}^{r_1}\frac{\rho dr}{12\epsilon(1-4\rho\epsilon)}\frac{4\epsilon+(1-12\rho\epsilon)r^2}{(-\epsilon+r^2-\rho r^4)^{1/2}}.\quad (F32)$$

Then, after some heavy algebra,

$$\int-\frac{1}{8}\frac{\mu'^2}{\mu}dr=\frac{3\rho}{8}-\frac{1}{12\epsilon}+\frac{10R^{-3/2}\rho^{1/4}R\sqrt{\rho}}{24\sqrt{2}}$$

$$-\frac{\rho^{1/4}R^{-3/2}}{24\sqrt{2}}\left(1+\frac{5}{4}\rho\epsilon-\frac{5}{4}(\sqrt{\rho})R\right)+Q.\quad (F33)$$

We have now determined Φ_C, the asymptotic expansion of Φ_{WKB} in region C:

$$\Phi_C \sim \frac{2^{1/4}\rho^{1/8}}{R^{1/4}}\left(1+\frac{5}{8}\rho\epsilon\right)\left[1+\frac{5}{8}(\sqrt{\rho})R\right]$$

$$\times\left(C_2 \exp\left\{i\left[\frac{R^{-3/2}\rho^{1/4}}{24\sqrt{2}}\left(5+\frac{25}{4}\rho\epsilon+\frac{15}{4}R\sqrt{\rho}\right)+P\right.\right.\right.$$

$$\left.\left.\left.+Q+\tfrac{3}{8}\rho-\frac{1}{12\epsilon}-\tfrac{1}{3}\sqrt{2}\rho^{-1/4}R^{3/2}[1-\tfrac{3}{2}(\tfrac{5}{6}\rho\epsilon+\tfrac{1}{2}\rho^{1/2}R)]\right]\right\}\right.$$

$$+C_3 \exp\{-i[\cdots]\}\Big),\quad (F34)$$

where P and Q are defined in Eqs. (F30) and (F32), respectively.

Region D. In region D, we substitute Eq. (F25) into the differential equation (F1) and transform the equation to

$$0=\left\{\frac{d^2}{dR^2}+\tfrac{1}{2}\rho^{-1/2}R\left[1-\rho\left(\frac{5}{2}\epsilon+\frac{5}{2}\frac{R}{\rho^{1/2}}\right)\right]\right\}\Phi(R).\quad (F35)$$

Equation (F35) must be solved to first order and Φ_D is its solution. We solve Eq. (F35) by finding a transformation of variable which to first order changes Eq. (F35) into an Airy equation.[29] The correct change of variables is

$$R=\rho^{1/2}[z+\rho(\tfrac{3}{2}+\tfrac{5}{6}\epsilon z+\tfrac{1}{2}z^2)].\quad (F36)$$

Then,

$$\Phi_D=\{\exp\tfrac{1}{2}\rho[z-\rho(\tfrac{5}{6}\epsilon+\tfrac{1}{2}z^2)]\}\chi.\quad (F37)$$

χ in Eq. (F37) satisfies this Airy equation to first order:

$$\{d^2/dz^2+\tfrac{1}{2}\rho z\}\chi=0.\quad (F38)$$

The solution to the Airy equation [Eq. (F38)] is

$$\chi(z)=[-\tfrac{1}{3}(18\rho^{-1})^{-1/3}z]^{1/2}$$

$$\times K_{1/3}(2(-z)^{3/2}(18\rho^{-1})^{-1/2}).\quad (F39)$$

[29] BMP, Vol. 2, Sec. 7.3.7, p. 22.

As in Sec. IV, to calculate the asymptotic behavior of Φ_D we need to use Eq. (4.31) which is[30]

$$K_{1/3}(e^{3\pi i/2}x) = -\tfrac{1}{2}i\pi[e^{i\pi/6}H_{1/3}^{(1)}(x)$$
$$+e^{-i\pi/6}H_{1/3}^{(2)}(x)]. \quad \text{(F40)}$$

Also, we need the asymptotic expansions of $H_{1/3}^{(1)}$ and $H_{1/3}^{(2)}$ to first order[31]:

$$H_{1/3}^{(1)}(x) \sim \frac{\sqrt{2}}{\sqrt{(\pi x)}} e^{i(x-5\pi/12)}\left(1+\frac{5}{i72x}\right) \quad \text{(F41a)}$$

and

$$H_{1/3}^{(2)}(x) \sim \frac{\sqrt{2}}{\sqrt{(\pi x)}} e^{-i(x-5\pi/12)}\left(1-\frac{5}{72ix}\right). \quad \text{(F41b)}$$

We combine Eqs. (F36), (F37), (F39), (F40), and (F41), and after some heavy algebra, we have the asymptotic expansion of Φ_D:

$$\Phi_D(R) \sim \frac{2^{-11/12}\pi^{1/2}3^{-1/3}\rho^{1/24}D}{R^{1/4}}\left(1+\frac{5\rho\epsilon}{24}+\frac{5R\sqrt{\rho}}{8}\right)$$

$$\times(\exp\{i[\tfrac{1}{3}\sqrt{2}\rho^{-1/4}R^{3/2}[1-\tfrac{3}{2}(\tfrac{5}{8}\rho\epsilon+\tfrac{1}{2}R\sqrt{\rho})]$$

$$-\tfrac{1}{4}\pi-(5/24\sqrt{2})\rho^{1/4}R^{-3/2}[1+\tfrac{3}{2}(\tfrac{5}{6}\rho\epsilon+\tfrac{1}{2}R\sqrt{\rho})]\}$$

$$+\exp\{-i[\cdots]\}). \quad \text{(F42)}$$

This completes the calculation of the asymptotic expansions for Φ_A, Φ_B, Φ_C, and Φ_D. It is necessary to asymptotically connect Φ_A with Φ_B and Φ_C with Φ_D as was done in the zeroth-order calculation in Sec. IV.

First, we match Φ_A in Eq. (F7) with Φ_B in Eq. (F24) and determine the ratio of C_2 to C_3:

$$\frac{C_2}{C_3} = (\tfrac{1}{8}r_0^2)^{\nu+1/2}e^{-i\pi/4}\frac{\Gamma(-\tfrac{1}{2}\nu)}{\Gamma(\tfrac{1}{2}+\tfrac{1}{2}\nu)}e^{i\epsilon/4}$$

$$\times\exp\left[i\rho\left(1+\frac{15}{64}\epsilon^2\right)\right], \quad \text{(F43)}$$

where ν is given in Eq. (F5).

Second, we match Φ_C in Eq. (F34) with Φ_D in Eq. (F42) and, once again, determine the ratio of C_2 to C_3:

$$\frac{C_2}{C_3} = e^{i\pi/2}\exp\left[-2i\left(P+Q+\frac{3\rho}{8}-\frac{1}{12\epsilon}\right)\right], \quad \text{(F44)}$$

where P and Q are given in Eqs. (F30) and (F32), respectively.

It only remains to calculate the integrals P and Q. Both integrals may be treated by substituting

$$z^2 = (r_1^2-r^2)/(r_1^2-r_0^2). \quad \text{(F45)}$$

After some algebra both P and Q are found to be linear combinations of $K(k)$ and $E(k)$. These are the complete elliptic integrals of the first and second kind.[32] $K(k)$ and $E(k)$ are defined by

$$K(k) \equiv \int_0^1 \frac{dz}{(1-z^2)^{1/2}(1-k^2z^2)^{1/2}} \quad \text{(F46a)}$$

and

$$E(k) \equiv \int_0^1 \frac{dz(1-k^2z^2)^{1/2}}{(1-z^2)^{1/2}}, \quad \text{(F46b)}$$

where in our case

$$k^2 \equiv 1-r_0^2/r_1^2. \quad \text{(F46c)}$$

Using Eq. (F46), P and Q may be written as

$$P = \frac{(\sqrt{\rho})r_1^3}{2}\left[\frac{2-k^2}{3}E(k)+2\left(\frac{k^2-1}{3}\right)K(k)\right] \quad \text{(F47)}$$

and

$$Q = \frac{\sqrt{\rho}}{12r_1\epsilon(1-4\rho\epsilon)}[4\epsilon K(k)+(1-12\rho\epsilon)r_1^2E(k)]. \quad \text{(F48)}$$

We expand $K(k)$ and $E(k)$ to first order for k near 1 by means of the following formulas[33]:

$$K(k) = \tfrac{1}{2}\pi \,_2F_1(\tfrac{1}{2},\tfrac{1}{2};1;k^2) \quad \text{(F49a)}$$

and

$$E(k) = \tfrac{1}{2}\pi \,_2F_1(-\tfrac{1}{2},\tfrac{1}{2};1;k^2). \quad \text{(F49b)}$$

We then expand the hypergeometric functions in Eq. (F49) to first order for k near 1[34]:

$$K(k) \sim \ln\frac{4r_1}{r_0}+\frac{r_0^2}{4r_1^2}\left(\ln\frac{4r_1}{r_0}-1\right) \quad \text{(F50a)}$$

and

$$E(k) \sim 1+\frac{r_0^2}{4r_1^2}\left(2\ln\frac{4r_1}{r_0}-1\right)$$

$$+\frac{3}{32}\frac{r_0^4}{r_1^4}\left(2\ln\frac{4r_1}{r_0}-\frac{13}{6}\right). \quad \text{(F50b)}$$

Equation (F2) allows us to write Eq. (F50) in terms of ρ and ϵ:

$$K(k) \sim \left(\ln\frac{4}{\sqrt{(\rho\epsilon)}}\right)\left(1+\frac{\rho\epsilon}{4}\right)-\frac{5\rho\epsilon}{4} \quad \text{(F51a)}$$

and

$$E(k) \sim 1-\frac{\rho\epsilon}{4}-\frac{77}{64}\rho^2\epsilon^2+\rho\epsilon\left(\frac{1}{2}+\frac{19}{16}\rho\epsilon\right)\ln\left(\frac{4}{\sqrt{(\rho\epsilon)}}\right). \quad \text{(F51b)}$$

Finally, we combine Eqs. (F47), (F48), and (F51) to

[30] BMP, Vol. 2, p. 5, Eq. (15) and p. 80, Eq. (43).
[31] BMP, Vol. 2, p. 85, Eqs. (1) and (2).
[32] BMP, Vol. 2, p. 317, Eqs. (1) and (2).
[33] BMP, Vol. 2, p. 318, Eqs. (5) and (6).
[34] For the expansion of $K(k)$ and $E(k)$ see Ref. 11.

get the first-order evaluation of P and Q:

$$P \sim -\frac{\epsilon}{4}\left(\ln\frac{4}{\sqrt{(\rho\epsilon)}}\right)\left(1+\frac{3\rho\epsilon}{8}\right)+\frac{1}{6\rho}-\frac{\epsilon}{8}+\frac{17}{128}\rho\epsilon^2 \quad \text{(F52)}$$

and

$$Q \sim \frac{1}{12\epsilon}-\frac{35\rho}{48}+\frac{3\rho}{8}\left(\ln\frac{4}{\sqrt{(\rho\epsilon)}}\right). \quad \text{(F53)}$$

Combining Eqs. (F52) and (F53) with (F44), we have

$$\frac{C_2}{C_3}=e^{i\pi/2}\exp\left\{i\left[\frac{\epsilon}{4}-\frac{1}{3\rho}+\rho\left(\frac{17}{24}-\frac{17}{64}\epsilon^2\right)\right.\right.$$
$$\left.\left.+\left(\ln\frac{16}{\rho\epsilon}\right)\left(\frac{\epsilon}{4}-\frac{3\rho}{8}+\frac{3\rho\epsilon^2}{32}\right)\right]\right\}. \quad \text{(F54)}$$

We have thus calculated two independent expressions for C_2/C_3. Setting these expressions in Eqs. (F43) and (F54) equal gives an even-parity version of Eq. (4.35) correct to first order instead of zeroth order as previously computed in Sec. IV. Thus,

$$\frac{\Gamma(\frac{1}{2}+\frac{1}{2}\nu)}{\Gamma(-\frac{1}{2}\nu)}=\exp\left[(\nu+\frac{1}{2})\ln\frac{2}{\rho}+i\left(\frac{5\pi}{4}+\frac{1}{3\rho}\right)\right.$$
$$\left.+i\rho\left(\frac{7}{24}-\frac{61E^2}{4}\right)\right], \quad \text{(F55)}$$

where

$$\nu=E-\frac{1}{2}+\frac{3}{2}i\rho(E^2+\frac{1}{4}).$$

This is the result we have sought. It is reassuring to observe that Eq. (F55) reduces to the zeroth-order calculation [Eq. (4.35)] if we neglect $\frac{3}{2}i\rho(E^2+\frac{1}{4})$ compared to $(E-\frac{1}{2})$ in ν and $\rho(7/24+E^2 61/4)$ compared to $5\pi/4$.

Considering the zeroth- and first-order results, it is tempting to conjecture that to all orders the WKB result corresponding to Eq. (F55) takes the form

$$\frac{\Gamma(\frac{1}{2}+\frac{1}{2}\nu(\rho))}{\Gamma(-\frac{1}{2}\nu(\rho))}=\exp\left\{[\nu(\rho)+\frac{1}{2}]\ln\frac{2}{\rho}\right.$$
$$\left.+i\left(\frac{5\pi}{4}+\frac{1}{3\rho}\right)+i\alpha(\rho)\right\}, \quad \text{(F56)}$$

where $\nu(\rho)$ and $\alpha(\rho)$ are power series in ρ:

$$\nu(\rho)=\sum_{n=0}^{\infty}\nu_n\rho^n, \quad \text{(F57)}$$

with $\nu_0=E-\frac{1}{2}$ and $\nu_1=\frac{3}{2}i(E^2+\frac{1}{4})$;

$$\alpha(\rho)=\sum_{n=1}^{\infty}\alpha_n\rho^n, \quad \text{(F58)}$$

with $\alpha_1=7/24-61E^2/4$.

APPENDIX G

In Sec. VI, the result of performing the integral $\int c\Phi_{\mathrm{WKB}}{}^2(z)dz$ was stated in Eq. (6.3). In this appendix, we demonstrate explicitly the evaluation of this integral which we call J. We will calculate J only for even-parity wave functions Φ. The odd-parity case is similar and presents no new difficulties.

We chose the contour C to be the straight line $z=re^{-i\pi/4}$, where r runs from $-\infty$ to ∞. Because the WKB solutions have definite parity about $r=0$, we simplify J to

$$J=2e^{-i\pi/4}\int_{r=0}^{\infty}dr\,\Phi_{\mathrm{WKB}}{}^2(re^{-i\pi/4}). \quad \text{(G1)}$$

In Eq. (G1) we break the region of integration into four pieces:

$$\text{(I)} \quad 0\leq r\leq\bar{r}_0,$$
$$\text{(II)} \quad \bar{r}_0\leq r\leq\bar{r}_1,$$
$$\text{(III)} \quad \bar{r}_1\leq r\leq r_2,$$
$$\text{(IV)} \quad r_2\leq r,$$

where

$$r_0<\bar{r}_0\ll\bar{r}_1<r_1<r_2. \quad \text{(G2)}$$

The $<$ sign in Eq. (G2) means that we disregard r_0 compared to $\bar{r}_0$ to zeroth order.

Φ_{WKB} is approximated by Φ_A [Eq. (4.12)] in region I, by the oscillating WKB solution [Eq. (4.16)] in region II, by Φ_D [Eq. (4.28)] in region III, and by the exponentially decreasing WKB solution [Eq. (4.5)] in region IV. The integrals in each of these regions must be treated separately using

$$J=J_{\mathrm{I}}+J_{\mathrm{II}}+J_{\mathrm{III}}+J_{\mathrm{IV}}. \quad \text{(G3)}$$

Region I. In region I, we evaluate

$$J_{\mathrm{I}}=2e^{-i\pi/4}\int_{r=0}^{\bar{r}_0}dr\,\Phi_A{}^2(re^{-i\pi/4}). \quad \text{(G4)}$$

Inserting Eq. (4.12), the definition of Φ_A, into Eq. (G4) we get

$$J_{\mathrm{I}}=2e^{-i\pi/4}C^2\int_{r=0}^{\bar{r}_0}[D_\nu(re^{-i\pi/4})+D_\nu(-re^{-i\pi/4})]^2dr, \quad \text{(G5)}$$

where $\nu=-\frac{1}{2}-\frac{1}{4}i\epsilon$ and $\epsilon=4iE$.

We expand the integrand in Eq. (G5) using identities of the parabolic cylinder functions[35] so that

$$J_{\mathrm{I}}=2e^{-i\pi/4}C^2\left[(1-e^{2\nu\pi i})\int_{r=0}^{\bar{r}_0}D_\nu{}^2(re^{-i\pi/4})dr\right.$$
$$+\left(\frac{\sqrt{(2\pi)}}{\Gamma(-\nu)}\right)^2 e^{\pi i(\nu+1)}\int_{r=0}^{\bar{r}_0}D_{-\nu-1}{}^2(re^{i\pi/4})dr$$
$$\left.+2(1+e^{\pi i\nu})\int_{r=0}^{\bar{r}_0}D_\nu(re^{-i\pi/4})D_\nu(-re^{-i\pi/4})dr\right]. \quad \text{(G6)}$$

---

[35] BMP, Vol. 2, p. 117, Eq. (7).

We evaluate the integrals in Eq. (G6) by introducing a new function F into Eq. (G4) as follows:

$$J_I = 2e^{-i\pi/4}\left\{\int_{r=0}^{\bar{r}_0} dr[\Phi_A{}^2(re^{-i\pi/4}) - F(r)]\right.$$

$$\left. + \int_{r=0}^{\bar{r}_0}\right\} dr\, F(r). \quad \text{(G7)}$$

$F(r)$ is the zeroth-order asymptotic approximation to those terms in $\Phi_A{}^2(re^{-i\pi/4})$ which would have divergent tails if integrated to $r=\infty$. This definition of $F(r)$ implies that a good approximation to J_I is

$$J_I \sim 2e^{-i\pi/4}\left\{\int_{r=0}^{\infty} dr[\Phi_A{}^2(re^{-i\pi/4}) - F(r)]\right.$$

$$\left. + \int_{r=0}^{\bar{r}_0} dr\, F(r)\right\}. \quad \text{(G8)}$$

All the integrations in Eq. (G8) can be done easily. Explicitly these integrals are

$$J_I \sim 2e^{-i\pi/4}C^2\left\{(1 - e^{2\nu\pi i})\int_{r=0}^{\infty} D_\nu{}^2(re^{-i\pi/4})dr\right.$$

$$+ \left(\frac{\sqrt{(2\pi)}}{\Gamma(-\nu)}\right)^2 e^{\pi i(\nu+1)}\int_{r=0}^{\infty} D_{-\nu-1}{}^2(e^{i\pi/4}r)dr + 2(1+e^{\pi i\nu})$$

$$\times \int_{r=0}^{\infty} dr[D_\nu(re^{-i\pi/4})D_\nu(-re^{-i\pi/4}) - F(r)]$$

$$\left. + \int_{r=0}^{\bar{r}_0} F(r)dr\right\}. \quad \text{(G9)}$$

Asymptotically, $D_\nu(re^{-i\pi/4})D_\nu(-re^{-i\pi/4})$ behaves as $[\sqrt{(2\pi)}/\Gamma(-\nu)]r^{-1}e^{i\pi/4}$ for large r.[36] However, if we were to choose the counterterm $F(r)$ to have this form, we would introduce a spurious pole at $r=0$. Therefore, we pick a form for $F(r)$ with the same asymptotic behavior at $r=\infty$ but with no pole in the region of integration. We thus define

$$F(r) \equiv \frac{1}{r+1}\frac{\sqrt{(2\pi)}}{\Gamma(-\nu)}e^{i\pi/4}. \quad \text{(G10)}$$

After rotating the contours in the complex plane by $\pi/4$ and $-\pi/4$, the first two integrals in Eq. (G9) become known forms.[37] In order to perform the third integral in Eq. (G9) which is

$$\int_{r=0}^{\infty}\left[D_\nu(re^{-i\pi/4})D_\nu(-re^{-i\pi/4})\right.$$

$$\left. - \frac{\sqrt{(2\pi)}}{\Gamma(-\nu)}(r+1)^{-1}e^{i\pi/4}\right]dr, \quad \text{(G11)}$$

we introduce a small positive ϵ into Eq. (G11) as follows:

$$\lim_{\epsilon\to 0}\int_{r=0}^{\infty}\left[D_{\nu-\epsilon}(re^{-i\pi/4})D_\nu(-re^{-i\pi/4})\right.$$

$$\left. - \frac{\sqrt{(2\pi)}}{\Gamma(-\nu)}\frac{1}{(r+1)^{\epsilon+1}}e^{i\pi/4}\right]dr. \quad \text{(G12)}$$

After rotating the contour in Eq. (G12) by $\pi/4$, the integrals become known forms.[38] We evaluate the integrals in Eq. (G12) and take the limit as $\epsilon\to 0$. After considerable simplification[39] the final result of this evaluation is

$$J_I \sim \frac{4C^2\sqrt{(2\pi)}\cos(\tfrac{1}{2}\nu\pi)e^{\nu\pi i/2}}{\Gamma(-\nu)}$$

$$\times[2\ln\bar{r}_0 - \psi(E+\tfrac{1}{2}) + \tfrac{1}{2}\pi\cot(\tfrac{1}{4} - \tfrac{1}{2}E)\pi], \quad \text{(G13)}$$

where $\psi(x) \equiv d\ln\Gamma(x)/dx$.

Region II. In region II, we evaluate

$$J_{II} \sim 2e^{-i\pi/4}\int_{r=\bar{r}_0}^{r_1} dr(-\epsilon + r^2 - \rho r^4)^{-1/2}2C_2C_3. \quad \text{(G14)}$$

To get this equation, we have substituted Eq. (4.16) into Eq. (G1) and squared the expression. In squaring, we have disregarded two small oscillatory terms because their contribution to the integral could only become significant if r were near r_0 or r_1. The choice of $\bar{r}_0$ and $\bar{r}_1$ as endpoints of the integration region prevents r from getting near r_0 or r_1.

To do the integral in Eq. (G14) we decompose the region of integration into three pieces:

$$J_{II} \sim 4C_2C_3 e^{-i\pi/4}\left(\int_{r=r_0}^{r_1} - \int_{r=\bar{r}_0}^{\bar{r}_0} - \int_{r=\bar{r}_1}^{r_1}\right)$$

$$\times dr(-\epsilon + r^2 - \rho r^4)^{-1/2}. \quad \text{(G15)}$$

By substituting $x^2 = (r_1{}^2 - r^2)/(r_1{}^2 - r_0{}^2)$ and $k^2 = 1 - r_0{}^2/r_1{}^2$, the first integral in Eq. (G13) is shown to be $K(k)$, the elliptic integral of the first kind.[40] The last two integrals are approximated by factoring $(-\epsilon + r^2 - \rho r^4) = \rho(r^2 - r_0{}^2)(r_1{}^2 - r^2)$. Combining these results gives

$$J_{II} \sim 4C_2C_3 e^{-i\pi/4}\left[-\ln\frac{2\bar{r}_0}{r_0} - \left(2 - \frac{2\bar{r}_1}{r_1}\right)^{1/2}\right.$$

$$\left. + \frac{1}{r_1\sqrt{\rho}}K(k)\right]. \quad \text{(G16)}$$

We now expand $K(k)$ for k near 1 [see Eq. (4.23b) for

---

[36] BMP, Vol. 2, pp. 122–123, Eqs. (1) and (2).
[37] BMP, Vol. 2, p. 122, Eq. (22).
[38] BMP, Vol. 2, p. 122, Eq. (21).
[39] BMP, Vol. 1, pp. 1–5 and 16.
[40] BMP, Vol 2, p. 317, Eq. (1).

this expansion] and find that the contribution from region II is

$$J_{II} \sim 4C_2 C_3 e^{-i\pi/4} [\ln(2/\bar{r}_0\sqrt{\rho}) - \rho^{1/4}\sqrt{2}(r_1 - \bar{r}_1)^{1/2}]. \quad (G17)$$

Regions III and IV. Using Eqs. (4.20), (4.28), and (4.29), we can write down the integral contribution from region III:

$$J_{III} = 2e^{-i\pi/4} \int_{r=\bar{r}_1}^{r_2} dr \frac{D^2}{3}$$

$$\times K_{1/3}^2 [2(18\sqrt{\rho})^{-1/2}(r-r_1)^{3/2}](18\sqrt{\rho})^{-1/3}(r-r_1). \quad (G18)$$

We notice that the contribution from region IV can be included in Eq. (G18) by increasing the upper limit of integration from r_2 to ∞. This is true because the $K_{1/3}$ Bessel function for region III and the WKB solution for region IV [Eq. (4.5)] have similar exponentially decreasing tails. Hence,

$$J_{III} + J_{IV} = 2e^{-i\pi/4} \int_{r=\bar{r}_1}^{\infty} dr \frac{D^2}{3}$$

$$\times K_{1/3}^2(2(18\sqrt{\rho})^{-1/2}(r-r_1)^{3/2})(18\sqrt{\rho})^{-1/3}(r-r_1). \quad (G19)$$

We simplify Eq. (G19) by substituting $s = r - r_1$:

$$J_{III} + J_{IV} = \frac{2e^{-i\pi/4}D^2(18\sqrt{\rho})^{-1/3}}{3}$$

$$\times \int_{s=\bar{r}_1-r_1}^{\infty} s\,ds\, K_{1/3}^2(2(18\sqrt{\rho})^{-1/2}s^{3/2}). \quad (G20)$$

Next, as we did in region I, we introduce a counterterm $G(s)$ in Eq. (G21) and extend the region of integration in Eq. (G22). This procedure facilitates the evaluation of the integrals.

$$J_{III} + J_{IV} = \frac{2}{3}e^{-i\pi/4}D^2(18\sqrt{\rho})^{-1/3}$$

$$\times \left\{ \int_{s=0}^{\infty} s\,ds\, K_{1/3}^2(2(18\sqrt{\rho})^{-1/2}s^{3/2}) \right.$$

$$+ \int_{s=\bar{r}_1-r_1}^{0} ds[sK_{1/3}^2(2(18\sqrt{\rho})^{-1/2}s^{3/2}) - G(s)]$$

$$\left. + \int_{s=\bar{r}_1-r_1}^{0} G(s)ds \right\}. \quad (G21)$$

This may be approximated by

$$J_{III} + J_{IV} \sim \frac{2}{3}e^{-i\pi/4}D^2(18\sqrt{\rho})^{-1/3}$$

$$\times \left\{ \int_{s=0}^{\infty} s\,ds\, K_{1/3}^2(2(18\sqrt{\rho})^{-1/2}s^{3/2}) \right.$$

$$+ \int_{s=-\infty}^{0} ds[sK_{1/3}^2(2(18\sqrt{\rho})^{-1/2}s^{3/2}) - G(s)]$$

$$\left. + \int_{s=\bar{r}_1-r_1}^{0} G(s)ds \right\}. \quad (G22)$$

Equation (G22) is a good approximation to Eq. (G21) because $G(s)$ is chosen to behave asymptotically as $K_{1/3}^2$ for s near $-\infty$.

We reduce the first integral Eq. (G22) to a known form by substituting

$$x = 2(18\sqrt{\rho})^{-1/2}s^{3/2}, \quad (G23)$$

and by using[41]

$$\int_0^{\infty} K_{1/3}^2(x)x^{1/3}dx = 2^{-5/3}3\Gamma^2(\tfrac{2}{3}). \quad (G24)$$

We simplify the second integral in Eq. (G22) by substituting Eq. (G23) again and by observing that[42]

$$K_{1/3}(xe^{\frac{1}{2}\pi i}) = (-\pi i/\sqrt{3})[J_{1/3}(x) + J_{-1/3}(x)]. \quad (G25)$$

Three Bessel function terms arise from plugging the square of Eq. (G25) into the second term in Eq. (G22). The techniques for integrating only one of these three terms will be presented here because the other two terms can be integrated similarly. Investigation of Eq. (G25) shows that in terms of the variable x the counterterm G is proportional to $x^{-2/3}$. As in region I, a limiting procedure must be used to do the counterterm integration as follows.

We insert a positive ϵ and the first of the three terms becomes

$$\lim_{\epsilon\to 0} \int_0^{\infty} \left[J_{1/3}(x)J_{1/3}(x(1+\epsilon))x^{1/3} \right.$$

$$\left. - \frac{(\cos x\epsilon)x^{-2/3}}{(1+\epsilon)^{1/2}\pi} \right]dx. \quad (G26)$$

The first integral in Eq. (G26) is a Weber-Schafheitlin integral.[43] The second may be evaluated by changing the contour. This gives a Γ function. The results are

$$\lim_{\epsilon\to 0} \left(2^{1/3}(1+\epsilon)^{-5/3} \frac{F(1,\tfrac{2}{3};\tfrac{4}{3};(1+\epsilon)^{-2})}{\Gamma(\tfrac{4}{3})\Gamma(\tfrac{1}{3})} \right.$$

$$\left. - \frac{\Gamma(\tfrac{1}{3})\epsilon^{-1/3}\cos\frac{1}{6}\pi}{\pi} \right). \quad (G27)$$

We transform[44] the hypergeometric function in Eq. (G27) as follows:

$$F(1,\tfrac{2}{3};\tfrac{4}{3};(1+\epsilon)^{-2}) = \frac{\Gamma(\tfrac{4}{3})\Gamma(-\tfrac{1}{3})}{\Gamma(\tfrac{1}{3})\Gamma(\tfrac{2}{3})}$$

$$\times(1+\epsilon)^2 F(1,\tfrac{1}{3};\tfrac{4}{3};-2\epsilon-\epsilon^2) + \frac{\Gamma(\tfrac{4}{3})\Gamma(\tfrac{1}{3})}{\Gamma(\tfrac{2}{3})}(1+\epsilon)^{2/3}$$

$$\times\left[1 - \frac{1}{(1+\epsilon)^2}\right]^{-1/3} F(\tfrac{1}{3},0;\tfrac{2}{3};-2\epsilon-\epsilon^2). \quad (G28)$$

[41] BMP, Vol. 2, p. 93, Eq. (36).
[42] BMP, Vol. 2, p. 5, Eq. (15), p. 80, Eq. (43), and p. 4, Eqs. (5) and (6).
[43] BMP, Vol. 2, Sec. 7.7.4, pp. 51–52.
[44] BMP, Vol. 1, p. 109, Eq. (4).

We simplify[39] Eq. (G28) and insert it into Eq. (G27). We can then take the limit as $\epsilon \to 0$ because the terms containing $\epsilon^{-1/3}$ cancel. The result is that

$$\lim_{\epsilon \to 0} \int_0^\infty dx\left(J_{1/3}(x)J_{1/3}((\epsilon+1)x)x^{1/3} - \frac{(\cos x\epsilon)x^{-2/3}}{\pi x(1+\epsilon)^{1/2}}\right) = -\frac{3\times 2^{1/3}}{\Gamma^2(\tfrac{1}{3})}. \quad (G29)$$

The second term $(J_{1/3}J_{-1/3})$ and the third term $(J_{-1/3}J_{-1/3})$ each contribute 0 to the second term in Eq. (G22).

Thus, the first two integrals in Eq. (G22) cancel. After substituting for G, we are left with the third term in Eq. (G22) which is

$$J_{\text{III}}+J_{\text{IV}} \sim -ie^{-i\pi/4}\frac{2D^2}{3}\left(\frac{\sqrt{\rho}}{3}\right)^{1/3}\pi \int_{s=\bar{r}_1-r_1}^0 x^{-2/3}dx, \quad (G30)$$

where $x = 2(18\sqrt{\rho})^{-1/2}s^{3/2}$. We evaluate Eq. (G30) and find that

$$J_{\text{III}}+J_{\text{IV}} \sim \pi D^2 e^{-i\pi/4}2^{7/6}\rho^{1/12}3^{-2/3}(r_1-\bar{r}_1)^{1/2}. \quad (G31)$$

We have now evaluated all of the integrals in Eq. (G1). Finally, we must relate the constants C, C_1, C_2, C_3, C_4, and D in Eqs. (G13), (G17), and (G31). To do so we use Eqs. (4.14)-(41.6), (4.32), (4.33), and (4.35) and show algebraically that

$$C^2 = \frac{\Gamma^2(\tfrac{3}{4}-\tfrac{1}{2}E)e^{-\pi iE/2}2^{-E}C_1^2}{(2\pi)^2}, \quad (G32a)$$

$$C_2C_3 = \frac{C_1^2}{\Gamma(\tfrac{1}{4}-\tfrac{1}{2}E)\Gamma(\tfrac{1}{4}+\tfrac{1}{2}E)}, \quad (G32b)$$

$$D^2 = \frac{\rho^{1/6}2^{4/3}3^{2/3}C_1^2}{\pi\Gamma(\tfrac{1}{4}+\tfrac{1}{2}E)\Gamma(\tfrac{1}{4}-\tfrac{1}{2}E)}. \quad (G32c)$$

We may pick an arbitrary value for C_1^2 because we are free to choose the over-all normalization of the original WKB wave function. We let

$$C_1^2 = \tfrac{1}{2}e^{i\pi/4}\Gamma(\tfrac{1}{4}+\tfrac{1}{2}E)\Gamma(\tfrac{1}{4}-\tfrac{1}{2}E). \quad (G33)$$

Substituting Eq. (G33) into Eq. (G32) and simplifying,[39] the results are

$$C^2 = \frac{\Gamma(-\nu)e^{-\pi iE/2}(\tfrac{1}{2}\pi)^{1/2}e^{i\pi/4}}{4\pi \cos\tfrac{1}{2}\pi\nu}, \quad (G34a)$$

$$C_2C_3 = \tfrac{1}{2}e^{i\pi/4}, \quad (G34b)$$

$$D^2 = (18\sqrt{\rho})^{1/3}e^{i\pi/4}/\pi. \quad (G34c)$$

Combining Eq. (G34) with Eqs. (G13), (G17), and (G31) shows that the contributions to J are

$$J_{\text{I}} \sim 2\ln\bar{r}_0 - \psi(E+\tfrac{1}{2}) + \tfrac{1}{2}\pi \cot(\tfrac{1}{4}-\tfrac{1}{2}E)\pi, \quad (G35a)$$

$$J_{\text{II}} \sim -2\ln\bar{r}_0 + \ln(4/\rho) - 2\rho^{1/4}\sqrt{2}(r_1-\bar{r}_1)^{1/2}, \quad (G35b)$$

$$J_{\text{III}}+J_{\text{IV}} \sim 2\sqrt{2}\rho^{1/4}(r_1-\bar{r}_1)^{1/2}. \quad (G35c)$$

Referring to Eq. (G3), we add together the three expressions in Eq. (G35) to find the total contribution to J which is

$$J = -\psi(E+\tfrac{1}{2}) + \tfrac{1}{2}\pi \cot(\tfrac{1}{4}-\tfrac{1}{2}E)\pi + \ln(4/\rho). \quad (G36)$$

Note that $\bar{r}_0$ and $\bar{r}_1$ have dropped out of this final expression. This completes the evaluation of J for even parity.

For odd parity the result is

$$J = -\psi(\tfrac{1}{2}+E) + \tfrac{1}{2}\pi\cot(\tfrac{3}{4}-\tfrac{1}{2}E)\pi + \ln(4/\rho). \quad (G37)$$

The only differences between the even- and odd-parity derivations occur in the algebraic manipulations in region I.